steel research international
www.steel-research.de

Uncertainty Quantification in Modeling Mold Heat Transfer in Steel Continuous Slab Casting with CON1D

*Scott Wells and Brian G. Thomas**

Computational models are powerful tools to quantify physical phenomena to gain valuable insights into a manufacturing process. Their accuracy is hindered, however, by uncertainty in the input data. Furthermore, when calibrating models with plant measurements, it helps to understand which variables have greatest effect on the critical model outputs. This work applies uncertainty quantification and sensitivity analysis to determine the most influential input parameters in the CON1D model of heat transfer and solidification in steel continuous casting with slag. Results show that the slag rim greatly affects heat flux near the meniscus, so control of its size is important. Heat flux and temperature down the mold depend greatly on velocity of the solid slag layer, and slag solidification temperature, which control the slag layer thickness, which in turn affects the interfacial resistance that controls heat transfer in the process. Scale formation on the mold coldface greatly increases mold temperatures. Based on the results presented here, models of heat transfer in continuous casting such as CON1D would benefit from plant measurements such as slag rim size and solid slag velocity, and lab measurements such as slag viscosity at lower temperatures, to better characterize this important slag property.

1. Introduction

Continuous casting (CC) is responsible for over 96% of global steel production[1] due to its high yield, high-quality products, and low operating cost. While the continuous casting of steel is a relatively mature metallurgical process, defect formation including breakouts,[2–5] inclusion entrapment,[6,7] cracking,[8–11] and segregation[12,13] persist despite considerable attention and improvements made over the past few decades. Further improvements require better fundamental and quantitative understanding of the complex inter-dependent solidification, thermodynamics, transport, and other phenomena that govern the formation of these defects. Accurate measurements in the harsh, high-temperature environment of the commercial continuous-casting process are difficult. With the rapid growth of computational modeling capabilities, numerical simulations have emerged as a critical component to provide this understanding.

Modeling of heat transfer and solidification in the mold region is the first step in predicting the complex phenomena that give rise to defects in continuous casting. Mold heat transfer governs meniscus solidification, which affects surface defects such as surface depression formation, deep oscillation marks, and slag or inclusion capture between primary dendrite arms. Surface depressions forming at the meniscus cause local drops in mold heat transfer, which lead to heat transfer nonuniformities, strain concentration, and crack formation.[9,14] Longitudinal surface cracks correlate strongly with meniscus heat flux, where both high and/or variable meniscus heat flux is detrimental.[15] The shell temperature history governs the steel microstructure, including dendrite arm spacing, grain size, and precipitation formation, which in turn controls steel ductility, mechanical properties, and thermal stresses that lead to crack formation and breakouts.[16] The shell thickness at mold exit is critical to contain the molten steel from excessive bulging, accompanying subsurface cracks or even breakouts, and to avoid thickness nonuniformities that may lead later to centerline bridging, liquid pocket entrapment, and centerline segregation.[17]

For these reasons, many computational models have been developed to quantify heat transfer phenomena in the mold region of steel continuous casting, which is illustrated in **Figure 1**.[18] Heat generated due to latent heat of solidification in the dendritic region or "mushy zone" between the solidus and liquidus temperature is transported to the flowing mold cooling water across thermal resistances consisting mainly of the solid steel shell, and the various layers of the interfacial gap between the mold and shell. In addition, at the meniscus, solidified mold slag forms a "slag rim", which controls initial solidification and heat flux at the meniscus. Lower down the mold, superheat is delivered to the dendritic region by the turbulent fluid flow in the liquid pool, which is largest where the jet impacts against the solidification front. The copper mold wall and the convection boundary layer at the mold cold face provide additional thermal resistances, which have important effects on mold temperature.

S. Wells, B. G. Thomas
Postdoctoral Fellow and Research Professor, Mechanical Engineering
Colorado School of Mines
Golden, CO 80401, USA
E-mail: bgthomas@mines.edu

The ORCID identification number(s) for the author(s) of this article can be found under https://doi.org/10.1002/srin.202400118.

DOI: 10.1002/srin.202400118

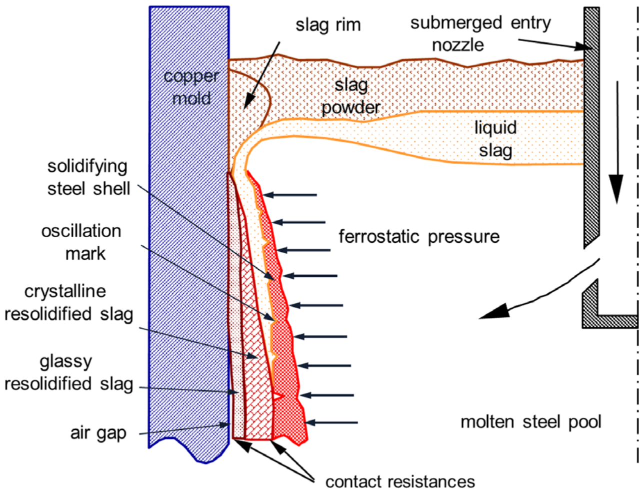

Figure 1. Schematic of phenomena in the steel continuous-casting mold. Figure adapted from.[18]

Computational simulation of continuous casting began in the 1970s with Lait[19] who developed a simple finite-difference model of steel shell solidification, and Brimacombe[20] who applied this model to caster design. Since then, with the rapid increase in computing power, more sophisticated models have been developed to simulate many phenomena in continuous casting, including heat transfer in the mold region, which are reviewed elsewhere.[21,22]

Some models of mold heat transfer include a sophisticated analysis of turbulent fluid flow in the mold. For example, Pfeiler et al.[23] applied such a coupled thermal-flow model to study how turbulent flow in the mold affects shell solidification and inclusion entrapment. Ramirez-Lopez has several publications on this topic[24–26] including a recent review on fluid flow driven phenomena in continuous casting and the ramifications of neglecting these phenomena.[27]

Some advanced models of mold heat transfer also feature a sophisticated treatment of heat transfer near the meniscus, which is greatly affected by the slag rim. Ramirez-Lopez et al.[24] conducted a sensitivity analysis on a flow model based in ANSYS-Fluent which included mold heat transfer and solidification. Their model used the volume of fluid (VOF) method and interface tracking to predict transient solidification behavior of the slag and shell in the mold region, and found several parameter-response relationships. In 2012, the same model was applied to study the formation mechanism of oscillation marks.[26] Initial solidification and oscillation mark formation at the meniscus has been further studied with VOF multiphase thermal-flow models, including the oscillating mold wall, by Ojeda et al.[28] Jonayat et al.[29] and Yan et al.[30]

Other advanced models of mold heat transfer have included the effects of shell shrinkage and mold distortion on the size of the interfacial gap between the shell and the mold. In 1988, Kelly et al.[31] applied a fully-coupled thermal-stress model to the continuous casting of round steel billets with oil lubrication, where the effects of steel shrinkage and hydrogen on the thickness and thermal conductivity of the gases in the air gap were found to be very important. Lee et al.[32] applied a similar model to predict temperature, stress, and crack initiation in the mushy zone. Park et al. applied such a model to investigate the effect of corner radius in billet casting, noting that air gap formation dominated the solidification behavior in the corners.[33] Song et al.[34] used a thermo-mechanical model to investigate interfacial air-gap and hot spot formation for a peritectic steel, which is prone to these problems associated with surface depressions. Similar analyses were conducted by Wang et al.[35] and Du et al.[36] using an inverse model approach. A 3D model of shell solidification in the mold region was used by Hebi et al.[37] to investigate mold–slag contact including the effects of friction.

The computational models of continuous-casting molds mentioned above vary in focus and complexity of the included physics, and most require extensive computational resources. The model studied here, CON1D, is a simple but comprehensive model of steel continuous casting which simulates transient heat transfer and solidification in a 1-dimensional slice through a steel shell, together with 2-dimensional steady state conduction in the copper mold. While CON1D can simulate the entire caster including primary cooling in the mold, secondary cooling, reheating, and beyond, this work focuses on solidification and heat transfer in the mold region. One benefit of CON1D and its relative simplicity is the high speed at which it executes to provide useful information including the heat flux leaving the shell, shell surface and interior temperatures, shell thickness, mold hot-face and cold-face temperature, cooling water heat up and average mold heat flux, solid and liquid slag thickness and velocity profiles, and more. Despite its simplicity, CON1D has been successfully verified against well-known analytical solutions[38] and more complex 3D models,[39–42] and has been extensively validated with plant measurements.[43–46] This model features extensive user control of relevant input parameters, thus allowing users to calibrate it to closely match real casters, and customize it to fit their needs.

Model calibration, verification, and validation play a vital role in the accuracy of computational models, including those of mold heat transfer in steel continuous casting. After verification by comparing with analytical solutions or other models, validation can be accomplished by: comparing with plant measurements such as the average mold heat flux (based on mold water heatup), mold thermocouple temperatures or shell thickness measurements along the length of the cast slab.[14,47–49] Calibration to match the measurements can be achieved through a trial and error approach,[49,50] or by inverse modeling[36] and can be augmented by comparing fast but simple models to high fidelity, but expensive computational models.[32,34,51] Calibration is easier knowing the relative importance of the casting conditions (input parameters to the model) on the heat transfer results (model outputs).

Like all models, however, success depends on accuracy of the model and its input parameters, which can be gained via good property data, accurate sensors to capture the processing conditions, and appropriate calibration to find good values of those model parameters that are difficult to measure. Uncertainly arises when choosing this input data, in addition to the assumptions and simplifications used in deriving and solving the model equations. Each source of uncertainty in turn can be divided into aleatoric (statistical) uncertainty resulting from natural variability that can be quantified by plant measurements, and epistemic (systematic) uncertainties resulting from a lack of knowledge or information. Uncertainty from both sources will propagate to the outputs of interest, and control the reliability of the model predictions.

The present work aims to quantify the influence of uncertainty in the input parameters on the most important output values of the CON1D 1-dimensional model of the continuous casting of steel, focusing on the mold region. Following the framework proposed by Wells et al.[52] the most impactful input parameters will be quantified, in order of importance. The results identify where: property measurement, plant sensing/measurement, model calibration, and model improvement endeavors should focus their efforts, as well as discovering which input parameters can already be measured with sufficient accuracy or have little impact on model predictions and do therefore not need of further attention.

Two different approaches will be taken to quantify the uncertainty in input parameters. Firstly, this uncertainty will be based on the natural variability estimated in the process for typical steady casting conditions, for best choices of state-of-the-art property data and comprehensive sensor/measurements possible at the plant. Secondly, considering the versatility of computational models and their wide-spread use in continuous casting plants, it is insightful to quantify the uncertainty arising from potentially nonoptimal parameter value selection by a non-expert, who may lack access to some of the plant data, or lack comprehensive understanding of all the many complex process phenomena involved in the casting operation, and/or details of the computational model equations. As such, the nonexpert user may experience a larger uncertainty on particular parameters, which in turn affects the variability of the results predicted by the model.

2. CON1D Model

CON1D simulates heat transfer and solidification during the continuous casting of steel.[18,38] The model is computationally efficient, running on a personal computer in just a few seconds, yet it features a realistic treatment of the phenomena illustrated in Figure 1.[18] These phenomena include superheat delivery to the solidification front from the liquid steel, the presence of a slag rim, 1-D conduction through the steel shell and interfacial gap, 2-D conduction in the copper mold, and finally convection heat transfer into the mold cooling water. It features a detailed treatment of heat transfer across the interfacial gap, including resistances due to the oscillation marks/surface depressions, contact resistances from air gaps, conduction and radiation through the solid and liquid slag layers, slag consumption and movement, and temperature-dependent properties. The following sections briefly explain how each of these phenomena is modeled.

2.1. Superheat Flux

During the continuous casting process, liquid steel flows into the mold at the tundish temperature or "pour" temperature (T_{pour}) which is assumed to be a constant in the present work, and must cool to the liquidus temperature before solidification can occur. Turbulent convection in the liquid pool results in an uneven distribution of the superheat to the solidification front. To account for these variations, a separate 3D computational fluid-dynamics (CFD) model should be run to find the fluid flow pattern in the mold, and the corresponding heat flux of superheat to the solidification front boundary. From a database of CFD model results for typical submerged entry nozzles flowing into slab casters with oversized, bifurcated, downward-angled ports, a superheat function given by Equation (1) is chosen here, which adjusts the database results according to the superheat temperature difference ΔT, and the casting speed V_c

$$q_{\text{sh}} = q_{\text{sh}}^{\text{o}} \frac{\Delta T_{\text{sup}}}{\Delta T_{\text{sup}}^{\text{o}}} \frac{V_c}{V_c^{\text{o}}} \tag{1}$$

This superheat flux is further adjusted according to the nozzle submergence depth, and incorporated into the 1D FDM heat conduction model of the solidifying shell via augmenting the latent heat.[53] Implementation of the superheat flux profile into CON1D is done computationally by enhancing the latent heat, as explained elsewhere.[54]

2.2. Slag Rim

CON1D allows the user to specify the thickness profile of the slag rim which may form above the point of maximum interfacial heat flux, where the molten steel first starts to solidify. The slag rim thickness at the location of peak heat flux and at the far-field liquid level are user input points, (which should be based on plant measurements), connected with a piece-wise linear interpolation. Larger slag rims typically arise when mold level fluctuations are more severe. The slag rim has an important effect on heat flux and depression formation at the meniscus, which in turn affects local mold temperatures, and behavior below the heat flux peak. In CON1D, the slag-rim effect on heat transfer is included as an extra resistance to heat flow across the interfacial gap according to its local thickness at that location down the mold.

2.3. Heat Conduction Through the Solidifying Steel Shell

Temperature in the solidifying steel shell is governed by the 1D transient heat conduction equation, given by Equation (2), which is solved in CON1D using an explicit finite-difference method in a 1D slice domain through the thickness of the steel shell, which moves down at the casting speed as illustrated in **Figure 2**.

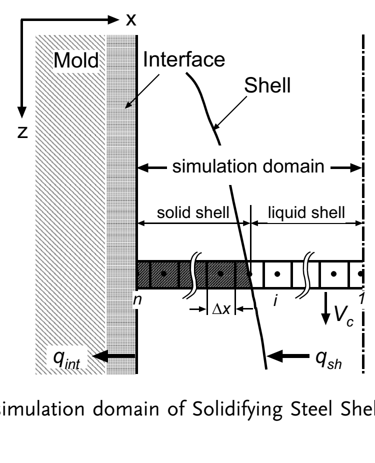

Figure 2. 1D simulation domain of Solidifying Steel Shell in CON1D.

$$\rho_{\text{steel}}\ Cp^*_{\text{steel}}\frac{\partial T}{\partial t}-k_{\text{steel}}\frac{\partial^2 T}{\partial x^2}-\frac{\partial k_{\text{steel}}}{\partial T}\left(\frac{\partial T}{\partial x}\right)^2=0;\ x>0 \tag{2}$$

where ρ_{steel} is the density, Cp^*_{steel} is the effective, temperature-dependent specific heat capacity given in Equation (3) which is augmented over the solidification-temperature range to account for the latent heat, which also includes the superheat, and k_{steel} is the temperature dependent thermal conductivity of the steel.

Heat is conducted from the solid steel shell surface at $\times = 0$ across the interfacial gap separating the shell from the mold as a heat flux boundary condition between the mold and shell domains, $q_{\text{int}} = -k_{\text{mold}}\ \partial T/\partial x$, as explained later. The initial condition at $t = 0$ is fixed just above the liquidus temperature at the meniscus. Liquid remains at this temperature at the far boundary, which is never reached by the solidifying shell.

Use of the 1D transient conduction equation relies on the assumption that heat conduction in the casting direction is negligible. This assumption is reasonable as the Péclet number is large due to the large advection associated with the downward casting speed.[14]

2.4. Steel Properties

CON1D allows the user to input the temperature- and composition-dependent density, thermal conductivity, and specific heat capacity and other steel properties including the liquidus and solidus temperatures, latent heat of fusion (L_f), surface emissivity ($\varepsilon_{\text{steel}}$), and the phase fraction curve, shown in **Figure 3**. As previously mentioned, an effective specific heat capacity is used which accounts for the latent and sensible heat and is governed by

$$C^*_p = C_p - L_f\frac{df_s}{dT} \tag{3}$$

where f_s is the phase fraction of the solid steel given graphically in Figure 3. Thus, latent heat is included into the model via an "enhanced specific heat". To overcome the numerical errors associated with the sudden property change, post-iterative corrections are applied to adjust the nodal temperatures to balance the latent heat evolved in the previous iteration before moving to the next time step, as explained elsewhere.[54]

The linear thermal expansion (CTE), needed for taper calculations, is calculated from the density using Equation (4)

$$\text{CTE} = \sqrt[3]{\frac{\rho_o(T_0)}{\rho(T)}} - 1 \tag{4}$$

where T_0 is the reference temperature.

2.5. Interfacial Gap Heat Transfer

Heat leaving the solidifying steel is conducted across the interfacial gap between the shell and the mold. This gap comprises the largest thermal resistance in the mold region of the continuous-casting process. To accurately quantify the heat flux across the gap (q_{int}), an effective heat transfer coefficient (h_{gap}) is calculated between the shell surface temperature (T_s) and the hot face of the copper mold (T_{mold}).

$$q_{\text{int}} = h_{\text{gap}}(T_s - T_{\text{mold}}) \tag{5}$$

The h_{gap} includes four distinct layers within the gap which vary down the length of the mold: solid and liquid slag, oscillation marks, and a potential air gap. It is calculated as follows, according to a network of resistors for these layers, as illustrated in **Figure 4**.

$$h_{\text{gap}} = 1\Bigg/\left(\left(r_{\text{contact}} + \frac{d_{\text{air}}}{k_{\text{air}}} + \frac{d_{\text{solid}}}{k_{\text{solid}}}\right) + 1\Bigg/\left(1\Bigg/\left(\frac{d_{\text{liquid}}}{k_{\text{liquid}}} + \frac{d_{\text{eff}}}{k_{\text{eff}}}\right) + h_{\text{rad}}\right)\right) \tag{6}$$

where d is the thickness and k is the thermal conductivity of each layer, r_{contact} is a contact resistance which captures the slag/shell

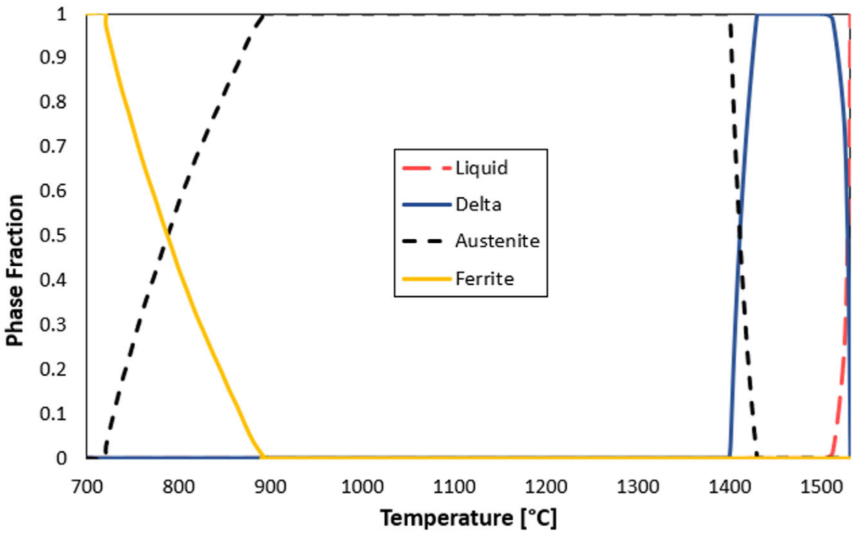

Figure 3. Steel phase fractions with temperature in the mold region.

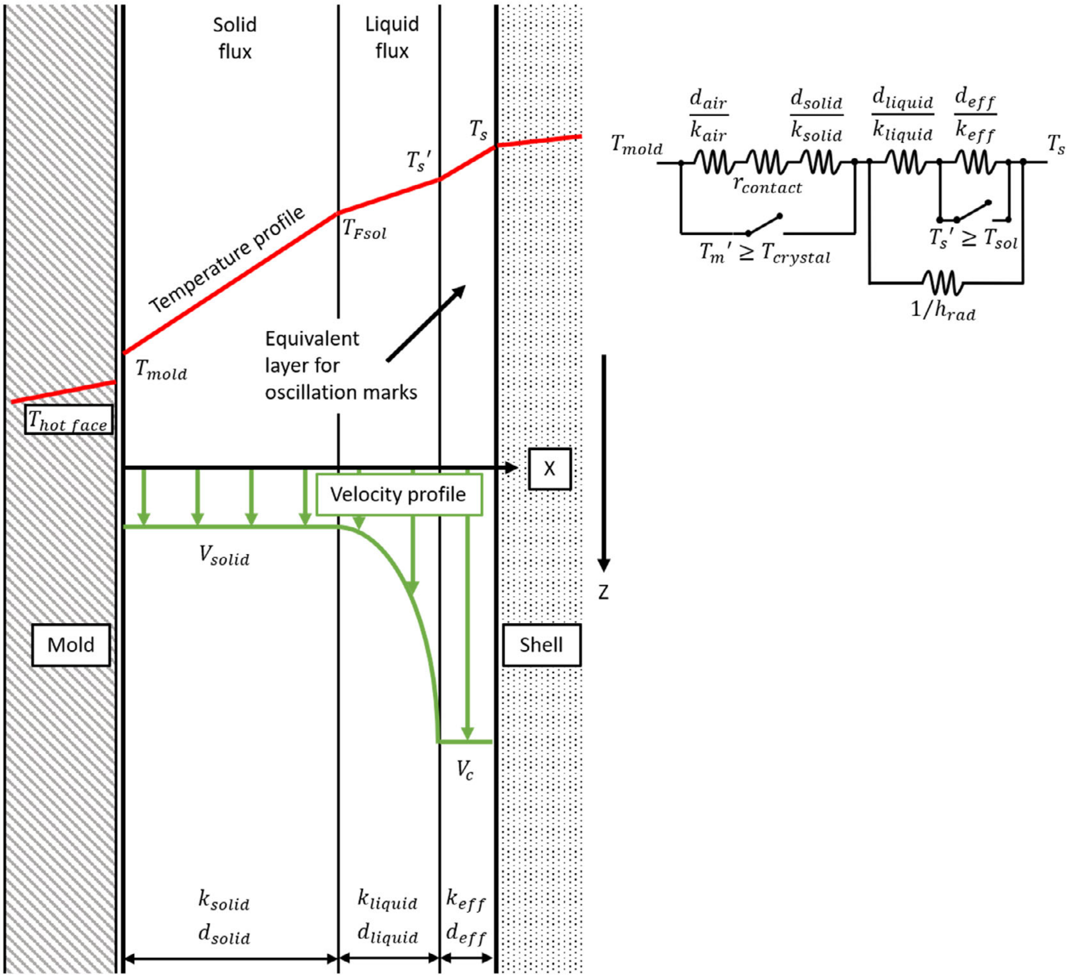

Figure 4. Schematic of temperature and velocity in the interfacial gap region, which is modeled as a resistance network.

and slag/mold interfaces, and h_{rad} is a heat transfer coefficient to account for radiation across the air gap, if present. An extra air gap often arises near the strand corner, where the solidified shell is strong enough to pull away from the mold, if the mold taper is inadequate, such that the thermally-distorted mold shape does not match with the shrinkage of the solidifying shell as it moves down the mold.[33] Except near the corners, such air gaps are negligible around most of the perimeter of slab casters, where the ferrostatic pressure maintains good contact between the shell and the mold.

The oscillation marks on the surface of the steel shell are approximated in CON1D with a "v"-shape according to the user-defined width (L_{mark}), and depth (d_{mark}). The distance between oscillation marks, L_{pitch} is calculated from the casting speed divided by the oscillation frequency. By simplifying oscillation marks to triangles, the volume-averaged oscillation mark depth can be calculated as

$$d_{osc} = \frac{0.5 L_{mark} d_{mark}}{L_{pitch}} \tag{7}$$

This d_{osc} depth is used to calculate the volume of slag carried downwards by the oscillation marks. The oscillation marks also impede heat transfer between the steel shell and the copper mold. By imposing a smaller effective gap thickness (d_{eff}), the appropriate effect on the interfacial heat flux can be calculated. This effective gap depth for heat transfer is calculated with Equation (8)

$$d_{eff} = \frac{0.5 L_{mark} d_{mark}}{(L_{pitch} - L_{mark})\left(1 + 0.5 \dfrac{d_{mark}}{d_{liquid} + d_{solid}} \dfrac{k_{gap}}{k_{mark}}\right) + L_{mark}} \tag{8}$$

where k_{gap} is the effective thermal conductivity of the gap given in Equation (9) and k_{mark} is the effective thermal conductivity of the oscillation marks, which depends on whether the depressions are filled with slag, hydrogen-enriched air, or a mixture.

$$k_{gap} = (d_{liquid} + d_{solid}) \Big/ \left(\frac{d_{solid}}{k_{solid}} + 1 \Big/ \left(\frac{k_{liquid}}{d_{liquid}} + h_{rad\_liquid}\right)\right) \tag{9}$$

Additionally, the semitransparent glassy slag next to the steel shell and the slag which is above T_{Fsol}, and therefore still liquid, experience radiative heat transfer, which is calculated by

$$h_{\rm rad} = \frac{m^2\sigma(T_{\rm s,K}^2 + T_{\rm Fsol,K}^2)(T_{\rm s,K} + T_{\rm Fsol,K})}{0.75a(d_{\rm liquid} + d_{\rm eff}) + \frac{1}{\varepsilon_{\rm slag}} + \frac{1}{\varepsilon_{\rm steel}} - 1}; T_{\rm mold} < T_{\rm Fsol} \quad (10)$$

where absolute temperatures (expressed in Kelvin) include $T_{\rm s,K}$, the shell surface temperature, and $T_{\rm Fsol,K}$ the final solidification temperature; m is the refractive index of the slag, and a is the absorption coefficient of the slag.

2.6. Mass and Momentum Balance in the Slag

During the continuous casting process, the slag flows down the mold as a solid layer, a liquid layer, and in the oscillation marks. Solid slag moves at a time-averaged velocity ($V_{\rm solid}$), which can be between zero and the casting velocity, and is governed by a user-input solid-slag velocity ratio (f_ν)

$$V_{\rm solid} = f_\nu \times V_{\rm c} \quad (11)$$

The liquid slag velocity in the liquid portion of the interfacial gap is governed by the Navier–Stokes equation for laminar Couette flow given by Equation (12) and decreases from the casting speed $V_{\rm c}$ on its hot side against the tips of the oscillation marks protruding from the shell surface to $V_{\rm solid}$ on its cold side against the solid slag layer. This liquid slag domain, $d_{\rm liquid}$, is illustrated by the non-constant region of the velocity profile in Figure 4.

$$\frac{\partial}{\partial x}\left(\mu\frac{\partial V_z}{\partial x}\right) = (\rho_{\rm steel} - \rho_{\rm slag})g; \quad x \in d_{\rm liquid} \text{ and } T_{\rm Fsol} < T < T_{s'} \quad (12)$$

where $T_{s'}$ is the average temperature of the slag at the oscillation mark tips.[42] The difference between the ferrostatic pressure from the liquid steel and the opposing weight of the slag flowing down the gap are accounted for by the body force that comprises the righthand side of Equation (12).

Liquid slag in the oscillation marks is carried downwards at the casting speed. After the shell surface temperature drops below $T_{\rm Fsol}$, so all of the slag across the gap has solidified, the slag in the oscillation marks is replaced by air, as explained elsewhere.[42]

2.7. Slag Properties

The temperature-dependent liquid slag viscosity depends on temperature according to the following exponential function

$$\mu(T) = \mu_{1300}\left(\frac{1300°{\rm C} - T_{\rm Fsol}}{T - T_{\rm Fsol}}\right)^n \quad (13)$$

Where $T_{\rm Fsol}$ and n are fitting parameters that should be based on experimental measurements, and μ_{1300} is the viscosity at 1300 °C. **Figure 5** presents the viscosity curve used in the present work, along with illustrating these parameters.

By integrating across the liquid region, and assuming that temperature varies linearly, an average liquid slag velocity across the interfacial gap ($\overline{V}_{\rm liquid}$) is calculated by

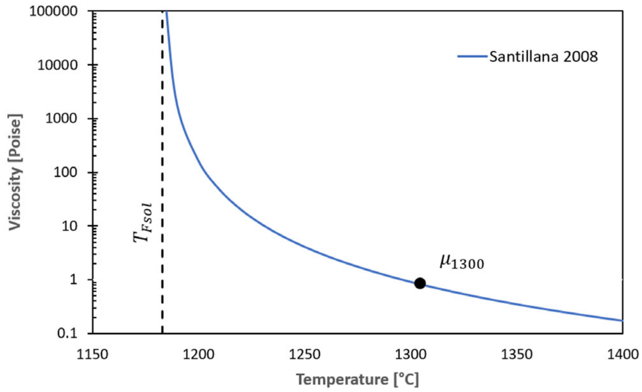

Figure 5. Viscosity curve for the present baseline case.

$$\overline{V}_{\rm liquid} = \frac{(\rho_{\rm slag} - \rho_{\rm steel})g d_{\rm liquid}^2}{\mu_{\rm s}(n+2)^2(n+3)} + \frac{V_{\rm c} + V_{\rm solid}(n+1)}{(n+2)} \quad (14)$$

where $\mu_{\rm s}$ is the viscosity of the liquid slag evaluated at the liquid layer/steel shell interface.

The powder/slag consumption rate $Q_{\rm slag}$ is important for accurately predicting interfacial gap heat transfer. This parameter is often expressed as mass of slag per unit surface area of the steel strand (kg m^{-2}).

$$Q_{\rm slag} = M_{\rm slag}\rho_{\rm steel}\frac{W \times N}{2(W+N)} \quad (15)$$

where $M_{\rm slag}$ is the input value of slag consumption per unit mass of the steel produced (kg ton^{-1}), typically based on plant measurements, W is the width and N the thickness of the steel slab. Slag is consumed by the moving solid layer, the moving liquid layer, and by the oscillation marks when filled with liquid slag, so the following mass balance is satisfied in CON1D everywhere down the mold

$$\frac{Q_{\rm slag}V_{\rm c}}{\rho_{\rm slag}} = V_{\rm solid}d_{\rm solid} + \overline{V}_{\rm liquid}d_{\rm liquid} + V_{\rm c}d_{\rm osc} \quad (16)$$

2.8. Copper Mold Heat Transfer

To account for conduction through the water-cooled copper mold, temperature in a 2-dimensional steady-state domain is calculated by solving Equation (17)

$$\frac{\partial^2 T}{\partial x^2} + \frac{\partial^2 T}{\partial z^2} = 0; \quad x \in x_{\rm mold} \quad (17)$$

for a constant thermal conductivity which is solved with a classic Fourier-series product solution with the hot face heat flux from the interfacial gap, $q_{\rm int}$ described earlier. The cold face heat flux, located at the roots of the water slots, is governed by the convective heat transfer coefficient due to the cooling water ($h_{\rm water}$), and the cooling water temperature ($T_{\rm water}$) boundary conditions. The remaining two boundary conditions are adiabatic. The 2D mold calculation domain extends horizontally across the solid mold portion of the mold thickness, (not including the water slots), x_{mold}, as shown in **Figure 6**. This mold domain extends vertically from the top of the mold to a user-defined distance below the meniscus, after which the temperature profile through the mold is nearly linear so a 1D calculation is sufficient.

In the horizontal plane through the mold, the important effect of water slot geometry on heat transfer through the mold into the cooling water is accounted for in CON1D in the undiscretized width direction by treating the copper between the cooling water channels as heat-transfer fins. As illustrated in Figure 6, the following heat transfer coefficient (h_{fin}) is applied to the solid mold T_{cold} plane

$$h_{\text{fin}} = \frac{h_{\text{w}} w_{\text{ch}}}{L_{\text{ch}}} + \frac{\sqrt{2 h_{\text{w}} k_{\text{mold}} (L_{\text{ch}} - w_{\text{ch}})}}{L_{\text{ch}}} \tanh \sqrt{\frac{2 h_{\text{w}} d_{\text{ch}}^2}{k_{\text{mold}} (L_{\text{ch}} - w_{\text{ch}})}} \quad (18)$$

where h_{w} is the heat transfer coefficient for the turbulent flow in the water channels, governed by the correlation by Sleicher and Rouse[55] in Equation (19). Mold geometry parameters $L_{\text{ch},}$ w_{ch}, and d_{ch} are the distance between parallel water channel centers, width and depth of the water channels, respectively, and k_{mold} is the thermal conductivity of the copper mold.

$$h_{\text{w}} = \frac{k_{\text{water}}}{D} \left(5 + 0.015 \times \text{Re}_{\text{water f}}^{C_1} \times \text{pr}_{\text{water w}}^{C2} \right) \quad (19)$$

In Equation (19), D is the equivalent diameter of the channel, Re is the Reynolds number, and Pr is the Prandtl number for the flowing water. Empirical constant c_1 is $0.88 - 0.24/(4 + \text{Pr}_{\text{water w}})$ and c_2 is $0.33 + 0.5e^{-0.6\text{pr}_{\text{water w}}}$.

Near the roots of the water channels, where the thermocouples are typically located, the temperature distribution is often complicated. To account for this, an offset distance can be applied to correct for the slight error in thermocouple temperature predictions, based on calibration of this CON1D reduced order model of the mold with a full 3D finite-element model of a representative segment of the mold, as discussed elsewhere.[46,56] In this work, the offset was set to 2.05 mm, based on calibration with a full 3D model of the mold, explained elsewhere.[46]

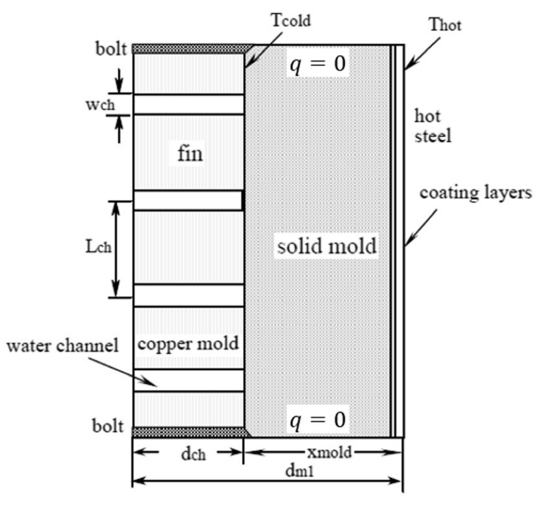

Figure 6. Water channel representation in CON1D.

3. Baseline Simulation

A simulation of a high-speed, funnel-mold, thin-slab caster from previous work by Santillana et al.[46] is chosen here as the baseline case to quantify the sensitivity of the model output predictions to uncertainty in the processing conditions, properties, and other input parameters. The baseline casting conditions are given previously[46] for new molds plates (0–5 mm mold wear), and the main input parameters are listed again in **Table 1–3**. The slag viscosity function is shown in Figure 5. The simulation focusses on a centerline slice down the narrow face of the strand, far from the corner, so the ferrostatic pressure maintains good contact between the shell and mold. This simplifies the interfacial heat transfer because there is no extra air gap.

The CON1D results were validated with plant measurements at the Corus (now Tata Steel) Direct Sheet Plant in IJmuiden, the Netherlands.[46] The measurements include average mold heat flux due to cooling water heatup and the temperatures of embedded mold thermocouples. The main CON1D output results are reproduced in **Figure 7**. These include profiles of mold temperatures, solidified shell thickness, shell surface temperature, and slag layer thickness with distance down the mold. Naturally, the results here agree exactly with the original results reported in ref. [46] and comparisons with plant measurements (Figure 7) show good agreement. These results are used as the baseline for the sensitivity analysis presented in the Section 6.

4. Input Parameters and Uncertainties

Many of the input parameters used within CON1D possess varying degrees of uncertainty, which arise from the measurement techniques used to find their values, and from natural variations

Table 1. Input parameter values with negligible uncertainty owing to accurate measurement availability (baseline case).

Parameter	Symbol	Units	Value
Casting speed	V_c	m min^{-1}	5.20
Pour temperature	T_{pour}	°C	1545
Nozzle submerged depth	d_{nozzle}	mm	150
Slab size (Thickness × Width)	–	mm	70 × 1420
Mold thickness (Narrow face)	–	mm	41.0
Oscillation frequency	–	cps	5.42
Oscillation stroke	–	mm	6.00
Water channel depth (WF, NF)	d_{ch}	mm	14.0, 17.0
Water channel width (WF, NF)	w_{ch}	mm	5.00, 9.00
Water channel spacing (WF, NF)	L_{ch}	mm	13.0, 21.0
Solidus temperature	T_{sol}	°C	1509
Liquidus temperature	T_{liq}	°C	1531
Fraction solid for shell thickness location	–	–	0.10
Thermocouple offset distance closer to hot Face	d_{offset}	mm	2.05

Table 2. Steel and slag compositions (baseline case).

Steel composition [wt%]		Slag composition [wt%]	
C	0.045	CaO	38.36
Mn	0.220	SiO_2	38.08
S	0.005	MgO	0.73
P	0.010	Na_2O	13.47
Si	0.015	K_2O	0.46
Cr	–	FeO	0.89
Ni	–	Fe_2O_3	0.89
Cu	–	NiO	–
Mo	–	Al_2O_3	3.27
Ti	–	TiO_2	0.01
Al	0.040	B_2O_3	–
V	–	F	8.60
N	–	free C	0.33
Nb	–	CO_2	0.23

in the casting conditions and parameters during the process. In this section, all input parameters and their associated uncertainties analyzed in this work are discussed and justified. Instances where a nonexpert user could reasonably but mistakenly introduce additional uncertainty are also detailed. Several parameters, including important parameters such as casting speed, have negligible uncertainty because they are easily measured with high accuracy. These are given in Table 1, and are not included in the investigation. A summary of all parameters and their associated uncertainties analyzed can be found in Table 3 presented in Section 3.

4.1. Mesh and Timestep

To ensure that the uncertainty in outputs of interest in this sensitivity analysis were independent of numerical errors, the grid spacing and timestep size were kept very small. Previous results from Zappulla et al.[14] found that a grid size of 0.1 mm and correspondingly small timesteps could reduce errors to 0.3% for stress phenomena, while predicted temperatures are more than an order of magnitude more accurate. As the present work is only concerned with the later, a constant grid spacing of 0.175 mm was used, which ensured that the mushy zone is always spanned by multiple grid points, and thus numerical errors were negligible. Similarly, a very fine timestep of 0.001 s (1 ms) was used to easily satisfy the Courant number criterion, to avoid any numerical issues for the explicit time-stepping algorithm in CON1D.[38]

Table 3. Parameter values and associated uncertainties for different users.

Parameter	Units	Baseline	Uncertainty Ranges		Reference
			Nonexpert	Sophisticated	
d_{rim}	mm	7	0–14	4–10	[57,58]
$f\nu$	–	0.104*z (m)	0.0–1.0	0.0–1.0	[59]
Scale	mm	0.0	0.2	0.1	–
Q_{slag}	kg m^{-2}	0.0589	0.050-0.068	0.053-0.065	[61]
k_{solid}	W mK^{-1}	1.00	0.85–1.15	0.87–1.13	[72–75]
K_{liquid}	W mK^{-1}	1.50	1.28–1.72	1.31–1.69	[72–75]
L_{mark}	mm	1.50	0.75–2.25	1.13–1.88	[64]
d_{mark}	mm	0.08	0.04–0.12	0.06–0.10	[64]
μ_{1300}	Poise	0.900	0.846–0.954	0.846–0.954	[65,66]
n	–	2.70	2.43–2.97	2.43–2.97	[67]
T_{Fsol}	°C	1183	1163–1203	1163–1203	[68]
$r_{contact}$	m^{2}K W^{-1}	1×10^{-7}	5×10^{-9}–5×10^{-4}	5×10^{-9}–5×10^{-4}	[38]
ρ_{steel}	Kg m^{-3}	7400	7252–7548	7252–7548	[70]
ρ_{slag}	Kg m^{-3}	2600	2548–2652	2548–2652	[70]
CTE_{mold}	1 k^{-1}	1.58–1.62 $\times 10^{-5}$	1.58–1.62 $\times 10^{-5}$	1.58–1.62 $\times 10^{-5}$	[71]
k_{steel}	W mK^{-1}	26.0	24.4–27.6	24.4–27.6	[72–75]
K_{mold}	W mK^{-1}	350	329–371	336–364	[72–75]
$C_{p\ steel}$	kJ kg K^{-1}	0.680	0.646–0.714	0.646–0.714	[77,78]
L_f	kJ kg^{-1}	271.0	260.2–281.8	260.2–281.8	[78]
k_{air}	W mK^{-1}	6.0×10^{-2}	2.4–9.6 $\times 10^{-2}$	5.82–6.18 $\times 10^{-2}$	[81]
ε_{mold}	–	0.50	0.45–0.55	0.45–0.55	[83]
ε_{steel}	–	0.80	0.72–0.88	0.72–0.88	[83]
ε_{slag}	–	0.90	0.70–1.00	0.70–1.00	[84]
a	m^{-1}	250	25–2500	25–2500	[85]

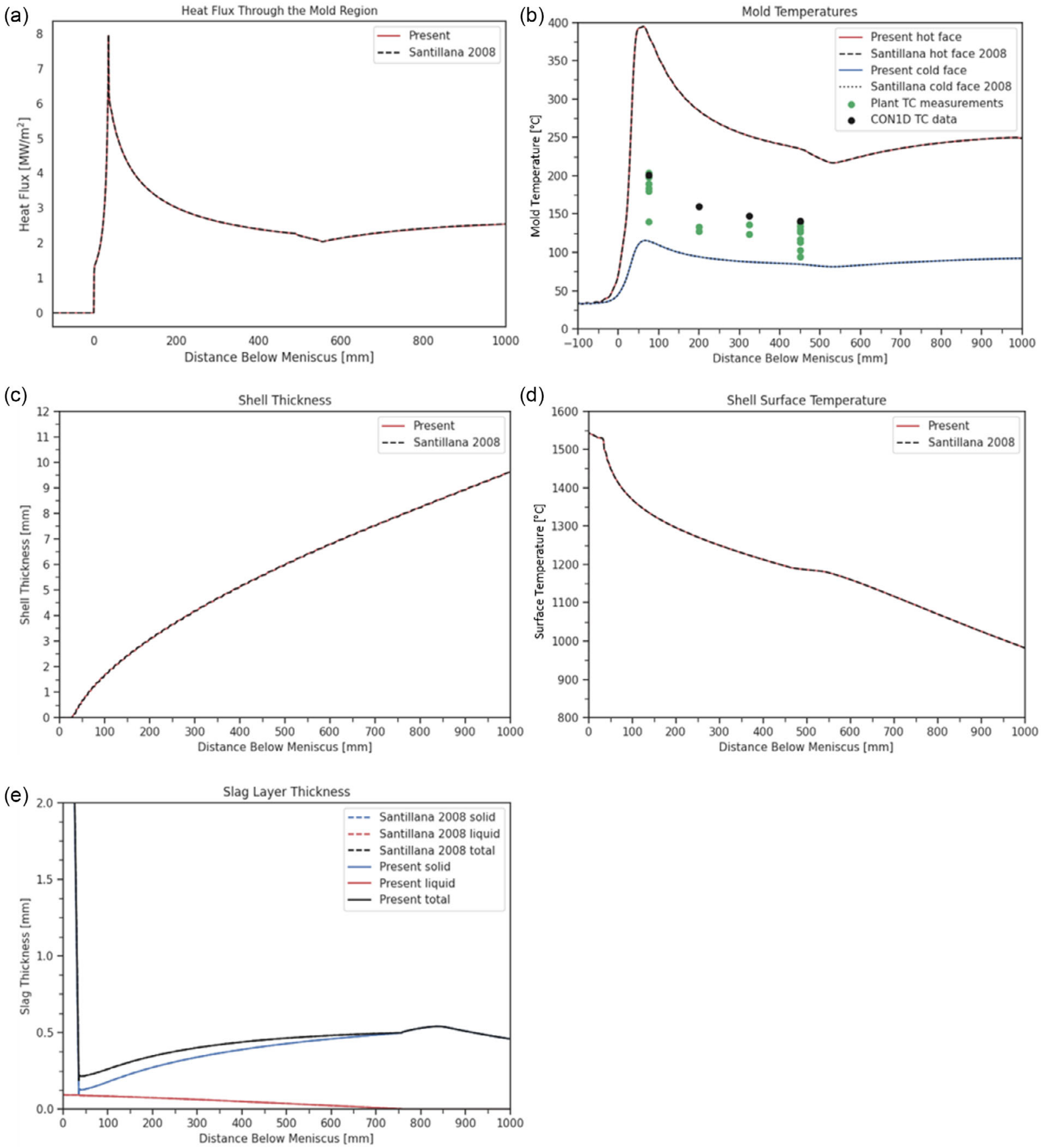

Figure 7. Comparison of present results with those of ref. [46] showing good agreement with past results and plant thermocouple data for a) heat flux, b) hot and cold mold face temperatures, c) shell thickness, d) shell surface temperature, and e) the slag layer thickness.

4.2. Slag Rim (d_{rim})

Thickness of the slag rim influences the heat flux near the meniscus and is therefore an important parameter when modeling heat transfer in the mold region. Several CON1D input parameters quantify the size and shape of the rim which forms above the meniscus. These depend on complex phenomena, such as level fluctuations in the turbulent liquid pool[57] and slag composition.[58] Measured slag rim thicknesses changed greatly for small variations in slag composition.[58] A nonexpert user would be unlikely to accurately quantify slag rim thickness. Slag cross-sections in ref. [58] show rim thickness variations of 10–15 mm so an uncertainty range of ±7 mm was assumed for the nonexpert user. A sophisticated user with a better controlled caster, better understanding of level fluctuations and slag composition effects, and access to accurate measurements of slag rim samples taken from the operating caster might be able to reduce this uncertainty to ±3 mm.

4.3. Solid Slag Layer Velocity Ratio (f_v)

The average velocity of the solid slag layer progressing down the mold wall expressed as a fraction of the casting speed, f_v, is difficult to measure, and it likely varies greatly with slag properties and casting conditions. Previous work suggests that f_v is on the order of 10% of the casting speed.[38,44,59] Given the lack of measurement data, the uncertainty in f_v is very high, and it is usually found via model calibration. If the solid slag layer attaches to the copper mold, then f_v is 0.0. At the other extreme, solid slag could attach to the steel shell traveling at the casting speed, so f_v is 1.0. In the present work, this full range is used for both nonexpert and sophisticated users. Because the baseline value of 0.05 was calibrated in previous work to match plant measurements,[46] the uncertainty range is very asymmetric.

4.4. Mold Scale Layer Formation

Scale forming on the copper mold surface may act to retard heat transfer between the mold cold face and the cooling water, causing the mold temperature to increase. This scale formation depends on precipitation of impurities in the mold cooling water combined with local boiling, if the mold cold face temperature is hot enough to allow it. Here, this effect was investigated for typical scale layers measured in service of 0.1 mm (expert user), and 0.2 mm for the non-expert. Although scale was not observed in the water channels of the mold under study, it is important to quantify the sensitivity of mold heat transfer to all parameters, including scale formation, both for stable plant operation and for model calibration.

4.5. Powder Consumption Rate (Q_{slag})

The powder consumption rate describes the rate of infiltration of liquid slag into the strand and is usually measured in bags ton^{-1} at the plant, and then converted to kg ton^{-1} or kg m^{-2}. The powder consumption rate depends on casting speed, viscosity, stroke, oscillation frequency, and flux solidification temperature.[60,61] Several relations to predict slag consumption exist in previous literature,[59–63] but are not well validated. Nevertheless, uncertainty in the consumption rates from plant measurements typically range from 10% to 15%[61] depending on the consistency of plant operations. Here, 10% is applied for a sophisticated user, which assumes measurements from a caster operating under steady conditions, whereas 15% is adopted for a nonexpert user, assuming estimates with a literature equation.

4.6. Slag Thermal Conductivity (k_{solid}, k_{liquid})

The crystalline/glassy nature of continuous casting slags generates additional uncertainty, compared with that of the metals. To account for this epistemic source of uncertainty, a value approximately twice that of reported values (12.5%) is expected for a sophisticated user. A nonexpert user might not correctly deduce the slag microstructure, or might not properly subtract the radiation component of heat transfer in flash diffusivity measurements, so a larger (15%) uncertainty was used.

4.7. Oscillation Mark Size (L_{mark}, D_{mark})

Oscillation mark size is affected by many processing parameters, including fluid flow in the mold, steel grade, casting speed, oscillation frequency, stroke, negative strip time, and slag behavior. Measurements of oscillation mark sizes using laser gauges are available in the literature and show variations up to 50% of the mean size, depending on the processing conditions.[64] Here, for a nonexpert user operating on an unoptimized caster or guessing values based on literature, the large uncertainty of ±50% reported by Lundkvist and Bergquist[64] is used. For a sophisticated user, the uncertainty should be based on variability of measurements of oscillation marks on actual as-cast slab samples for a given set of stable casting conditions, which should have a tighter range, ≈(±25%).

4.8. Slag Viscosity (μ_{1300}, n, T_{Fsol})

The present model of slag viscosity requires three parameters. The flux viscosity at 1300 °C is the simplest, most commonly measured parameter and its uncertainty has been estimated by McCauley et al.[65] and Persson et al.[66] via rotational viscometry measurements for many mold flux compositions to fall between 3% and 6%, so 6% is used here.

The exponent in the present flux viscosity model is analogous to the viscous activation energy so the uncertainty in previous work on activation energy was investigated. For example, Kobatake et al.[67] reported variations in the viscous activation energy for a ternary alloy system of ≈10%, which is used as the uncertainty in n here.

The final slag solidification temperature T_{Fsol} is the third parameter in the present viscosity model and is undoubtably the most difficult to quantify. Viscosity data in previous literature rarely exceed 1000 Poise, due to limitations in viscometer accuracy at higher viscosities, but the viscosity exceeds 10^8 Poise for liquid transforming to solid, which is needed for T_{Fsol}, Predictions of final solidification temperature for crystalline slags are likely more accurate, because crystallization typically occurs over a narrow temperature range, near the break temperature, where viscosity suddenly increases to ≈1000 Poise, and measurements are readily available. For example, Sridhar et al.[68] estimated uncertainty in break temperature measurements of ±20 k. Thus, for the crystalline slag investigated in the present study, ±20 k was taken as the uncertainty for T_{Fsol}.

For glassy slags, however, the viscosity increases much more gradually with decreasing temperature, so the slag acts as a lubricating fluid over a much wider temperature range, extending many hundreds of degrees below the break temperature. Meng et al.[42] measured T_{Fsol} to be 850 °C, which was ≈250 °C below the break temperature of 1100 °C for a glassy continuous-casting slag. Such measurements are rare. It is therefore difficult to estimate the final solidification temperature for glassy slags, so their uncertainties are very large, at least ±100 K, especially for a nonexpert (based on ref. [68]).

Another source of uncertainty, for the nonexpert, arises from the difference between the powder composition, which is readily measured and provided by the powder producer, and the actual composition of the liquid and solidifying slag in the caster, such as given in Table 2, which is somewhat different, and requires separate measurements of plant samples taken from the mold during casting.

4.9. Slag Layer/Mold Contact Resistance ($r_{contact}$)

A contact resistance between the solid slag layer and copper mold arises due to the thin average air gap that characterizes the surface roughness of the resolidified mold flux against the mold hot face wall. Cho et al.[69] reported contact resistances up to $\approx 10^{-3}$ m^2 K W^{-1}, based on surface roughness measurements up to $\approx$0.15 mm. Many previous computational investigations of steel continuous casting neglect this roughness effect or assume negligibly small contact resistance, such as 10^{-9} m^2 K W^{-1} by ref. [38].

Lacking actual measurements of the resolidified slag roughness, a better method to estimate this contact resistance is to assume that the liquid slag will continue to flow, as it is pushed against the mold wall by the ferrostatic pressure transmitted through the steel shell, until the hot side of the effective gap reaches the slag solidification temperature, $T_{Fsol.}$[50] The gap thickness that defines the contact resistance can then be calculated from the temperature drop across the gap, ($T_{Fsol} - T_{Mold\text{-}hotface}$), given a reasonable estimate of the air gap conductivity.

Considering the difficulties of quantifying slag solidification temperature, and/or effective air gap thickness as a function of processing conditions and distance down the mold, as well as the prevalence of the negligible air gap assumption, the present work assumes a large uncertainty range for contact resistance that spans several orders of magnitude from 5×10^{-9} to 5×10^{-4} m^2 K W^{-1}.

4.10. Density and Coefficient of Thermal Expansion (ρ_{steel}, ρ_{slag}, CTE_{mold})

Density can be measured via pushrod dilatometry, Archimedean methods, electrostatic levitation, and other methods to a high degree of accuracy. Reported uncertainties for solid and liquid materials are less than 2%, even at temperatures as high as 3000 K.[70] Furthermore, density has a relatively linear effect on heat transfer. Thus, both a sophisticated and nonexpert user could find a good value of this property for common steel grades with very little uncertainty, such as by taking the program defaults.[38] The uncertainty in thermal expansion (CTE) using Equation (4) would be similarly low. Alternatively, CTE can be calculated using dilatometry where a 1–2% uncertainty is reported in the literature.[71]

4.11. Steel and Mold Thermal Conductivity (k_{steel}, k_{mold})

The uncertainty in thermal conductivity can be derived from thermal diffusivity measurements using techniques such as flash diffusivity. Uncertainty calculations in thermal conductivity of metals have been reported to be on the order of 4–6% at temperatures as high as 3000 K[72–75] for common industrial alloys such as copper and steel, so 6% is used in the present work for k_{mold} and k_{steel}. In this work, where steel conductivity depends on temperature, uncertainty is applied only to the constant in the polynomial. The temperature-dependent components remain constant.

4.12. Steel Specific Heat Capacity and Latent Heat of Fusion (Cp_{steel}, L_f)

Data for the specific heat capacity and the latent heat of fusion for the solid-liquid phase change for metals and alloys are generally measured using calorimetry methods. Reported uncertainties at elevated temperatures range from 3 to 5%,[76,77] so 5% was used here for Cp_{steel}. Similarly, uncertainty in the latent heat of fusion was estimated at 3% for 316L stainless steel,[78] and this should not change much with steel composition. Similar to the thermal conductivity, the uncertainty in specific heat was restricted to the constant term in the temperature-dependent relation, which is graphed in **Figure 8**.

4.13. Air Thermal Conductivity (k_{air})

Conductive heat transfer across the air gaps created by oscillation marks in continuous casting is accounted for in the model, so uncertainty in the thermal conductivity of the gas in these gaps must be quantified. A nonexpert user might simply take measurements of the thermal conductivity of air. A sophisticated user would understand that vaporizing mold powder components could generate hydrogen, which increases the air conductivity, as shown in **Figure 9**,[79] based on a mixture equation.[80] Thus, the uncertainty for the nonexpert user could be large (+/−10% H_2 centered around 20%), whereas a sophisticated user, with access to the air-gap composition would only be limited by the uncertainty in the measurement technique for conductivity of a known gas, which is only 3%.[81]

4.14. Emissivity (ϵ_{mold}, ϵ_{steel}, ϵ_{slag})

Emissivity of copper and copper alloys for the mold depends on the extent of surface roughness and oxidation. Zhang et al.[82] measured the emissivity of oxidized metals up to 1073 K with reported uncertainty of only 2.9%, but this was in a highly-controlled environment. In a more realistic representation of continuous casting environment, is the work by Fernandez et al.[83] reported up to 10% uncertainty in emissivity of oxidized industrial metals (including copper).

Emissivity of the slag surface depends on slag composition, thickness, and crystallinity. While emissivity can be measured using spectroscopy with an integrating sphere, experimental data for continuous casting slags is scarce. One study of crystalline slags reported uncertainty in emissivity of 22%.[84] Considering expected differences between glassy and crystalline slags, expected uncertainty would be higher, especially for nonexpert users.

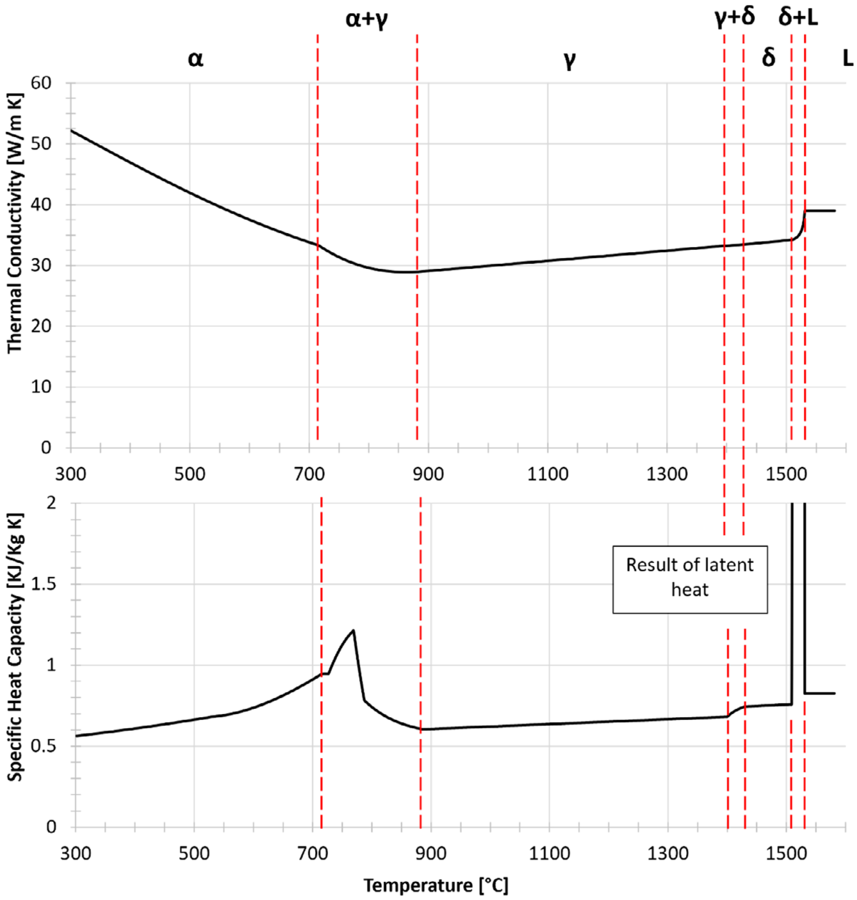

Figure 8. Temperature dependent thermal conductivity and specific heat capacity for the base-case steel.

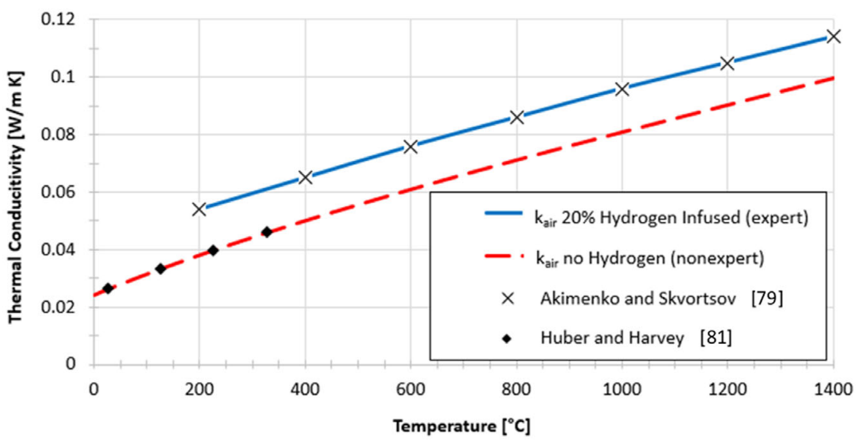

Figure 9. Temperature dependent curves for the thermal conductivity of air with and without infused hydrogen from evaporated moisture. A nonexpert user may not account for this effect.

4.15. Slag Absorption Coefficient (*a*)

The absorption coefficient of the slag depends greatly on wavelength, spanning over several orders of magnitude depending on the wavelength considered, for both crystalline and glassy slags.[85] Because CON1D requires a single constant value of *a*, both the nonexpert and sophisticated user are resigned to use an uncertainty of ± a full order of magnitude. As with the solid slag layer velocity ratio, the uncertainty bounds are asymmetric around the baseline value.

5. Outputs of Interest

The influence of uncertainty in the parameter values presented in the previous section on model accuracy is investigated here in the context of several important outputs of interest, which were selected for their relevance to defect formation. These outputs include: 1) shell thickness at mold exit, which is important for breakout prevention, strand bulging, internal crack formation, and centerline segregation due to bridging; 2) shell surface temperature, heat flux at the meniscus, and peak heat flux, which are all related to the formation of surface defects and cracks (especially longitudinal cracks); 3) shell surface temperature and heat flux at mold exit, which are important for surface cracks, (especially transverse cracks); and 4) mold hot and cold face temperature, which are important for mold life.

6. Sensitivity Analysis Results

To quantify the effects of uncertainty in the model input parameters, two extra simulations are needed for each model input parameter. These are for the upper and lower limits (estimating $\pm 3\sigma$), which are presented in Table 3, and are repeated for both sophisticated and nonexpert users, while keeping all other parameters constant. Variations in the results quantify the sensitivity of the model predictions to the uncertainty in each input parameter. This enables identification of those parameters with uncertainties that most influence model behavior. Finding ways to reduce the uncertainty in these most sensitive parameters would provide the greatest improvement to model reliability. These are also the parameters where attention should focus most when calibrating the model to match plant measurements. At the other extreme, identifying low sensitivity parameters is also useful because this prevents the wasting of resources to investigate model input parameters that would ultimately provide minimal gain.

7. Results and Discussion

The sensitivity analysis described above was executed with CON1D for the base case typical thin-slab caster conditions[46] to determine the importance of the uncertainty range of each model input parameter on predicted results for six key outputs related to mold heat transfer, including two representative values each of shell thickness, surface temperature, and mold heat flux. For readability, only parameters with a resulting uncertainty greater than 1% are included. **Figure 10–14** illustrate the sensitivities for a nonexpert user. Similarly, **Figure 15–19** present results for a sophisticated user, familiar with both the CON1D model and the casting process phenomena, and with understanding or access to measurements regarding the unavoidable variations in these input variables due to natural changes in process conditions during steady casting in an optimized caster. Negative percent changes correspond to decreasing from the baseline to the minimum value in the uncertainty range, and produce the blue dark-shaded rectangular boxes in the results variables. When such a decrease in the input parameter causes an increase in the heat-transfer output under consideration, then the dark blue box appears on the right. Increases from the baseline produce light-red boxes, which would appear on the right if the output result also increased. Important parameters are discussed in detail in the following subsections. Parameters which control the thermal properties of the interfacial gap are the most important, so a separate section is devoted to each of the most important of those parameters. Other sections include the mold scale layer, (which affects the mold/cold-side resistance) and finally the steel thermal properties, (which affect the thermal resistance of the steel shell).

7.1. Insignificant Parameters

Many input parameters were found to have low sensitivity, meaning that they contribute negligible propagation of uncertainty to the model results. These parameters are listed in **Table 4**, where "low sensitivity" is defined by a change from the baseline predictions for all outputs of interest by less than 1%. There are three causes for low observed sensitivities: 1) the input parameter can be measured to a high degree of certainty, so there is negligible uncertainty to propagate, 2) the input parameter has relatively low uncertainty, and sufficiently small impact on heat transfer that propagation is small, and 3) the input parameter has a large uncertainty, but the model is very insensitive to the parameter.

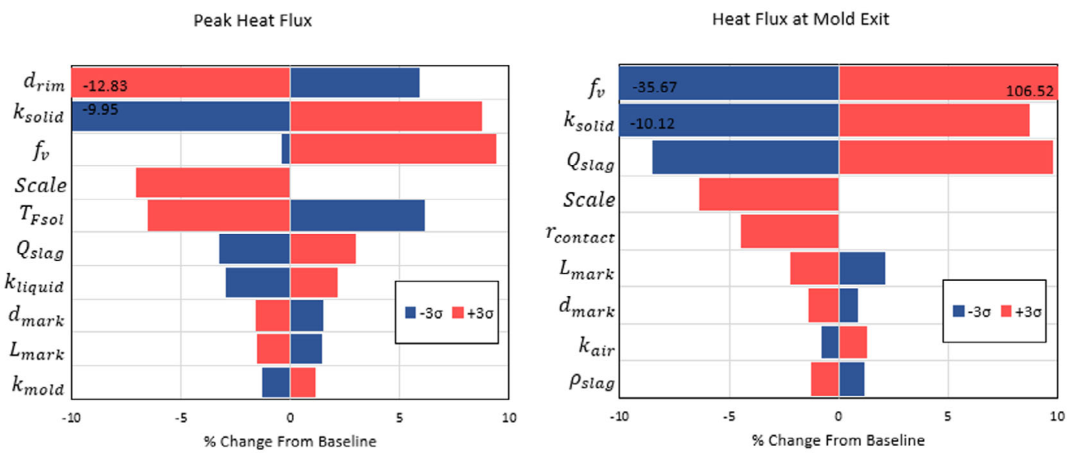

Figure 10. Heat flux sensitivity predictions (at peak and at mold exit) for a nonexpert user.

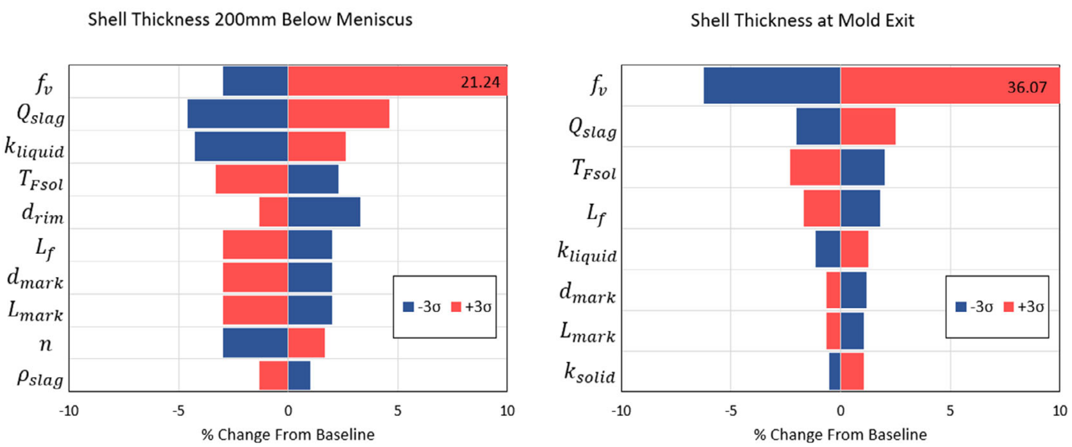

Figure 11. Shell thickness sensitivities (near meniscus and at mold exit) for a nonexpert user.

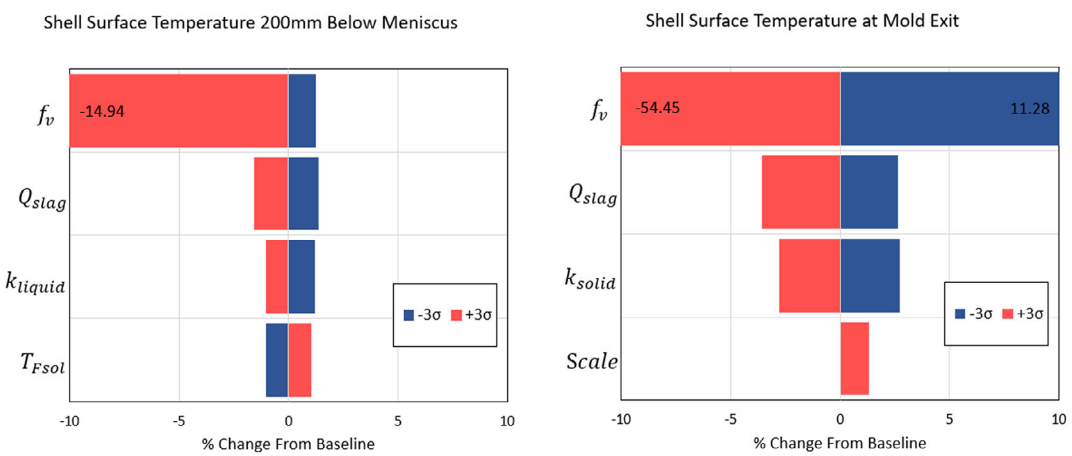

Figure 12. Steel shell surface temperature sensitivities (near meniscus and at mold exit) for a nonexpert user.

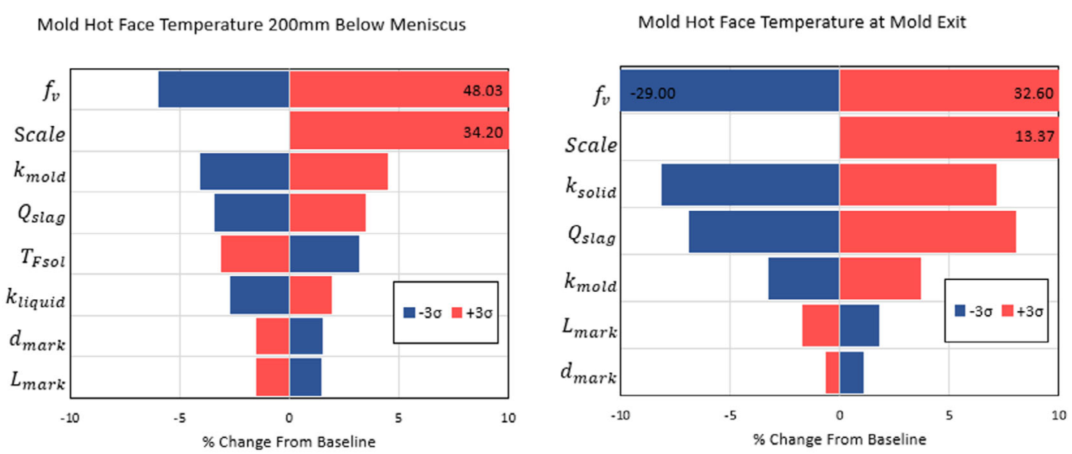

Figure 13. Mold hot face temperature sensitivities (near meniscus and at mold exit) for a nonexpert user.

Casting speed is an example of a type 1) low-sensitivity parameter. Heat transfer varies greatly with casting speed, but this parameter is known to such a high degree of certainty, that the uncertainty has negligible effect. Similarly, mold geometry parameters can be measured with high accuracy, so although they greatly influence mold temperature, they also have low sensitivity.

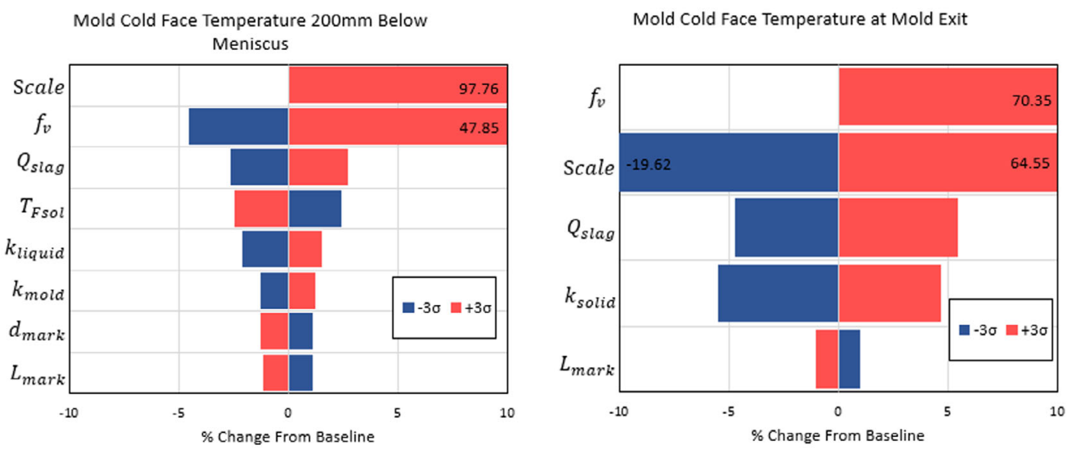

Figure 14. Mold cold face temperature sensitivities (near meniscus and at mold exit) for a nonexpert user.

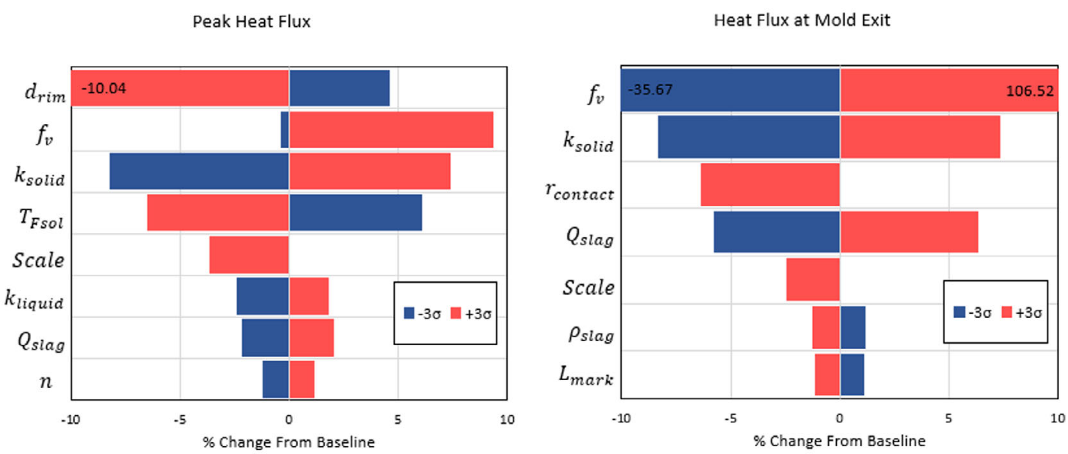

Figure 15. Heat flux sensitivities (at peak and at mold exit) for a sophisticated user.

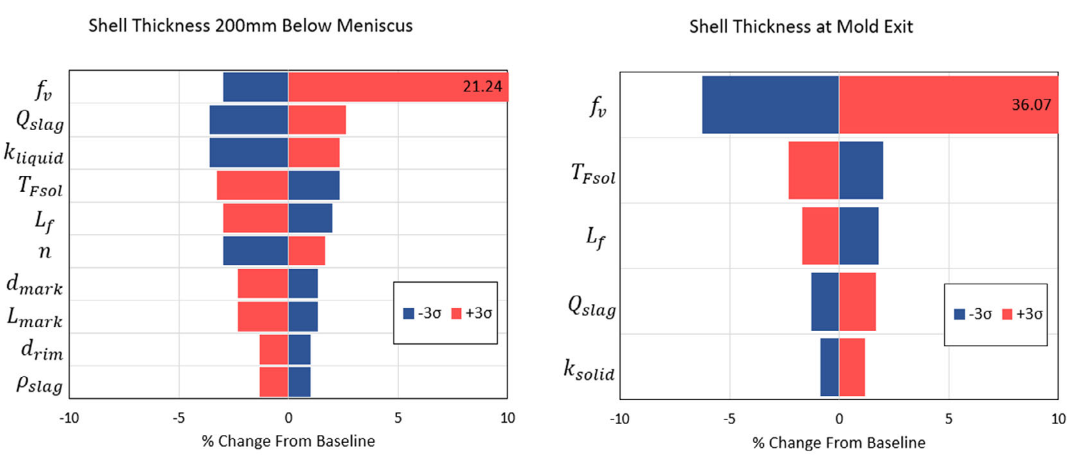

Figure 16. Shell thickness sensitivities (near meniscus and at mold exit) for a sophisticated user.

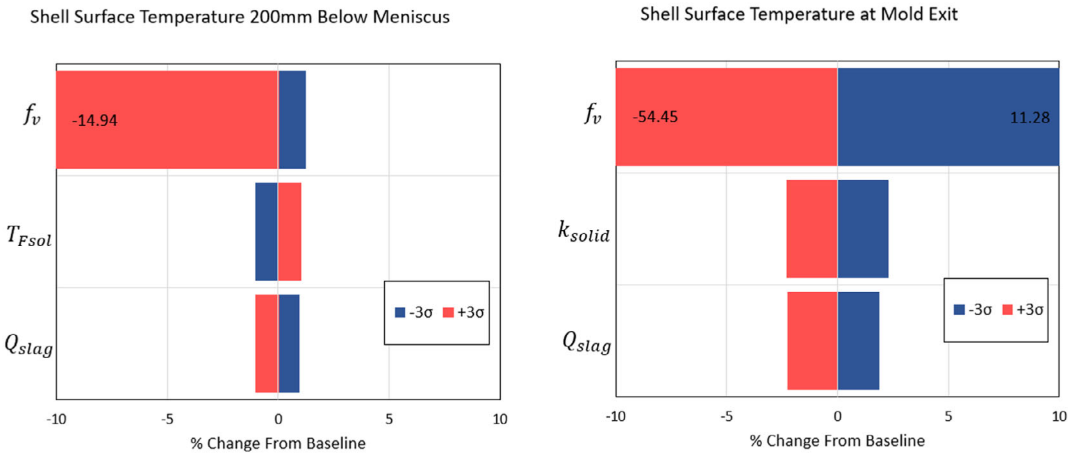

Figure 17. Steel shell surface temperature sensitivities (near meniscus and at mold exit) for a sophisticated user.

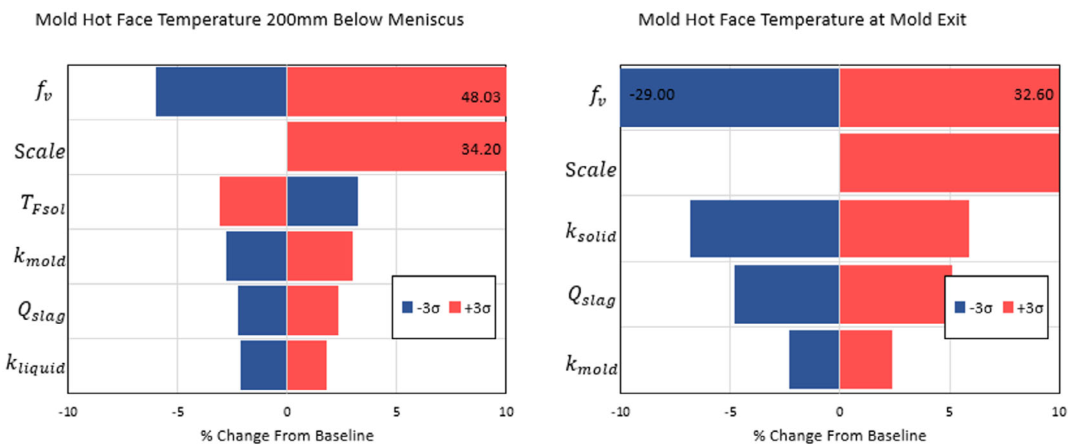

Figure 18. Mold hot face temperature sensitivities (near meniscus and at mold exit) for a sophisticated user.

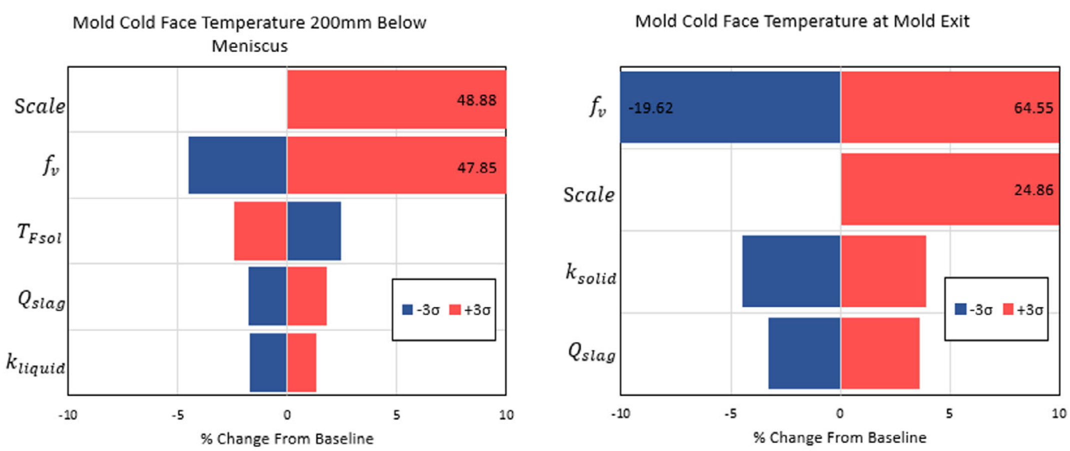

Figure 19. Mold cold face temperature sensitivities (near meniscus and at mold exit) for a sophisticated user.

Table 4. Low sensitivity parameters.

Parameter	Symbol	Units	Baseline value	Highest sensitivity	
				Parameter	Value [%]
Input parameters with negligible uncertainty (Type 1)					
Casting speed	V_c	m min^{-1}	5.20	–	–
Pour temperature	T_{pour}	°C	1545	–	–
Nozzle submerged depth	d_{nozzle}	mm	150	–	–
Strand thickness	–	mm	70	–	–
Slab width	W	mm	1420	–	–
Mold thickness	–	mm	41.0	–	–
Oscillation frequency	–	cps	5.42	–	–
Oscillation stroke	–	mm	6.00	–	–
Water channel depth (WF, NF)	d_{ch}	mm	14.0, 17.0	–	–
Water channel width (WF, NF)	w_{ch}	mm	5.00, 9.00	–	–
Water channel spacing (WF, NF)	L_{ch}	mm	13.0, 21.0	–	–
Initial cooling water temperature	T_w	°C	35.0	–	–
Equivalent diameter of water channel (h_w boundary condition)	D	mm	14.0	–	–
Low model sensitivity resulting from low uncertainty (Type 2)					
Steel liquidus temperature	T_{liq}	°C	1531	–	–
Steel solidus temperature	T_{sol}	°C	1509	–	–
Mold thermal expansion	CTE	K^{-1}	1.30×10^{-05}	–	0.0
Mold emissivity	ε_{mold}	–	0.50	–	0.0
Steel density	ρ_{steel}	Kg m^{-3}	7400	Shell thickness	−0.53
Steel specific heat capacity	$C_{p\ steel}$	kJ kg K^{-1}	0.68	Peak heat flux	0.43
Steel thermal conductivity	k_{steel}	W mK	26.0	Peak heat flux	0.53
Steel emissivity	ε_{steel}	–	0.80	Peak heat flux	0.43
Flux viscosity at 1300 °C	μ_{1300}	Poise	0.90	–	0.0
Low model sensitivity despite large parameter uncertainty (Type 3)					
Flux absorption coefficient	a_{flux}	m^{-1}	250	Peak heat flux	−0.33
Flux emissivity	ε_{flux}	–	0.90	Shell thickness	0.98
Air thermal conductivity	k_{air+H2}	W mK^{-1}	0.06	Peak heat flux	1.27

Type 2 low-sensitivity parameters include the steel properties (density, specific heat, thermal conductivity, and latent heat), and slag viscosity at 1300 °C. These parameters can be measured with reasonable accuracy and do not have much effect on the results for typical low-C steels.

Type 3 low-sensitivity parameters include emissivities, and absorption coefficient. Even though these parameters may have large uncertainty, they have very little effect on the mold heat transfer results. Air conductivity, for example, has little effect because the ferrostatic pressure maintains good shell contact with the mold, so the air gap is always very small, and only contributes like a contact resistance.

Low-sensitivity parameters of all types 1–3 are listed in Table 4. The sensitivities of all results parameters to these input parameters are all <≈1%. Considering their low sensitivities, searching for more accurate values or better operational control of any of these three types of input parameters appears not to be worth the effort, relative to focusing on the other parameters discussed in the next sections. An exception might be the liquidus and solidus temperatures. Although their uncertainties have negligible effect on heat transfer, the mushy-zone temperature range is very important to crack formation.

7.2. Slag Rim

The results show that slag rim size is the most important parameter affecting peak heat flux. This finding is logical, as the peak heat flux occurs near the meniscus where the slag thickness is smallest, and heat is most easily conducted out of the steel into the copper mold. Thus, small changes in slag rim size have a great effect on peak heat flux. This finding means that better understanding of how the slag rim forms and behaves would enable better control of peak heat flux, and the accompanying surface defects. It also suggests that formation of excessive slag rims might be a major reason why mold level fluctuations are detrimental.

Recent work has shown, with the help of high-density Fiber–Bragg sensors in the meniscus region, that the peak heat flux and start of solidification may be displaced significantly below the far-field liquid level, and that an extended slag rim is the likely cause. For a controlled caster with consistent slag powder composition and smaller level fluctuations, there should be less variation in slag rim size, and consequently less variations in peak heat flux. This should decrease surface defects associated with meniscus heat flux variations.

In addition to their dominating influence on peak heat flux, the uncertainties in slag rim size parameters have a small influence on shell thickness near the top of the mold. They are otherwise relatively low-sensitivity parameters.

7.3. Solid Slag Layer Velocity Ratio

The average velocity of the solid slag layer down the mold wall, relative to the casting speed, f_v, has a large uncertainty, as this parameter is rarely documented. Thus, f_v shows the largest sensitivity for most heat transfer results in the mold, in Figure 10–19, with exception to the peak heat flux and mold face temperatures. If the solid slag layer moves down the mold quickly, then its thickness is small. Heat then conducts easily through the interfacial gap, producing higher heat flux, a thicker steel shell, lower shell surface temperature, and higher mold face temperatures. Alternatively, if f_v is small, then the slower-moving solid slag layer leads to a thicker slag layer, for a given consumption rate, so provides a more insulating gap, resulting in lower heat flux, and a thinner, hotter steel shell, but lower mold face temperatures due to the slower heat transfer through the gap.

Indirect measurements of mold temperature suggest that mold slag moves very intermittently. There is likely some downward movement during every oscillation cycle, especially during the negative strip time, when the mold is moving downward faster than the casting speed. Other observations of "saw-tooth" temperature profiles suggest a rapid movement of the slag layer, moving near to the casting speed, as the entire sheet of mold slag is removed from the mold, followed by a slow buildup over 5–10 min.[86] Sometimes very long time scales exist, where the slag sticks to the mold wall, as evidenced by observations of startup slag in the mold even after several hours of casting.[87]

The CON1D model here focuses on the smaller of these time scales, (one residence time of the shell in the mold), where there are no experimental measurements. Thus, the dominant behavior of f_v observed in Figure 10–19 is due to both the high sensitivity of mold heat transfer to the solid slag-layer velocity ratio, and the high uncertainty in this important parameter.

7.4. Mold Scale Layer Formation

Formation of a scale layer on the mold cold face during continuous casting acts as a resistance to heat transfer from the mold cold face to the cooling water. As explained in Section 3 and 4.4, the baseline simulations were all executed with no scale layer. The sensitivity analysis was conducted using only upper bounds (specifically a scale layer of 0.1 mm for the sophisticated user and 0.2 mm for the non-expert) which results in the asymmetry observed in Figure 13, 14, 18, and 19.

Results in Figure 14 and 19 show that while a scale layer has a negligibly-small effect on the heat flux and solidifying steel shell, it has a profound effect on the mold temperature, particularly on the cold face where it dominates over all other sources of uncertainty. This finding is very significant, because if the cold face temperature exceeds the boiling temperature of the cooling water, then steam could form in the water channels, greatly decreasing the cold face heat transfer coefficient. This would encourage any impurities in the water to plate out, leading to further scale formation, and further decrease in heat extraction. Thus, once scale formation gets started, it is likely to worsen, owing to the high sensitivity of the mold temperature to scale formation and the increased likelihood of boiling. Furthermore, small changes in scale formation can lead to large variations in heat extraction and mold temperature.

The corresponding similar increases in copper hot face temperatures, quantified in Figure 13 and 18, could lead to increased wear, spalling, and other damage to the hot face copper and its coatings, particularly in high-speed casting operations where the mold hot face temperature is already high. This could lead to surface defects, such as longitudinal cracks, on the adjacent strand surface. These results show that control of water purity and mold temperature is vital to avoid scale formation, in order to extend mold service life and to lessen strand surface defects due to deteriorating mold hot face condition caused by excessive mold temperature.

7.5. Slag Consumption Rate

The consumption rate of the melted powder directly affects the slag layer thickness, so this parameter has similar influence on mold heat transfer phenomena as discussed above for solid slag velocity. However, this parameter is relatively easy to measure in the plant, and reasonable correlations exist to predict powder consumption, so its uncertainty is mainly aleatoric and easier to quantify. The smaller uncertainty range of slag consumption leads to similar but much lower sensitivities to all heat transfer output parameters as the solid slag layer velocity ratio. Thus, its importance can be reliably modeled and understood, making it easier to control and predict its effects in the plant.

7.6. Slag Thermal Conductivities

The results in Figure 10–19 show that the thermal conductivity, of the solid and liquid slag layers (k_{solid}, k_{liquid}), is very influential on all outputs of interest. It is not surprising that slag thermal conductivity has higher sensitivity than steel, because its uncertainty is significantly higher (see Section 2.3) and the interfacial gap is the most important thermal resistance in the process. Closer to the meniscus, the liquid slag conductivity shows higher sensitivity, (for the shell thickness and surface temperature), because there is more liquid slag higher in the mold. Progressing down the mold, liquid-slag thermal conductivity becomes steadily less important, while solid-slag thermal conductivity becomes increasingly important, mirroring the relative phase fractions in the interfacial gap. In contrast, the solid-slag conductivity shows a very high sensitivity for heat flux, even high in the mold, which is due to the large solid-slag rim above the meniscus, to which peak heat flux has the largest sensitivity.

7.7. Oscillation Mark Size

Model predictions were consistently sensitive to oscillation mark size (both d_{mark} and L_{mark}) for all outputs of interest, with a typical change in the baseline cases of ±1–4%. These depressions act as small periodic insulators (whether filled with air or slag) which decrease heat transfer across the interfacial gap. Larger oscillations mark (d_{mark} or L_{mark}) thus cause lower heat flux, in Figure 10 and 15, and thinner shell thickness, in Figure 11 and 16. Through proper caster optimization and flux powder selection, oscillation mark size can be minimized to improve both process variations and model reliability, as demonstrated by the reduced sensitivity for a sophisticated user.

7.8. Slag Viscosity

The temperature-dependent slag viscosity is defined here by three parameters (μ_{1300}, n, T_{Fsol}). Firstly, the results show a negligible sensitivity to the viscosity at 1300 °C (μ_{1300}) so this uncertainty can be ignored. This is due to both the relatively high accuracy of plentiful measurement data, and its small effect on mold heat transfer. In contrast, variability in mold heat transfer is quite sensitive to uncertainty in the final solidification temperature of the slag (T_{Fsol}) and also somewhat to the viscosity exponent (n) which defines how the viscosity behaves between the two points. For the thin slab caster studied here, a crystalline slag was used, so the uncertainty is lower, as explained earlier and given in Table 3. If the slag were glassy or had unknown crystallinity, mold heat transfer would have been far more sensitive to these two parameters.

The model outputs are very sensitive to the second slag viscosity parameter, slag solidification temperature, T_{Fsol}. A higher slag solidification temperature results in a thicker solid slag layer near to the meniscus which decreases heat flux near to the peak by >6%. This important finding helps to confirm and explain the common industry practice of using high-basicity crystalline slags with high solidification temperature when casting peritectic steel grades which are sensitive to depressions. The thicker solid slag layer increases the total resistance of the interfacial gap, thus making the heat flux less sensitive to the further variations caused by the deep oscillation marks and depressions. Variable heat flux at the meniscus is associated with crack formation.

This effect of higher T_{Fsol} decreasing heat flux near the meniscus generally decrease with distance down the mold. Some exceptions/variations occur where the liquid slag runs out and the slag layer becomes fully solid, which occurs further up the mold with higher T_{Fsol}. This parameter has little effect on heat flux near mold exit, where the slag is fully solid. However, the general decrease in mold heat flux greatly affects all other model output parameters, as expected. Shell thickness decreases, shell surface temperature increases, and mold temperature toward the top of the mold decrease. Thus, slag solidification temperature is the most important slag viscosity parameter influencing mold heat transfer and deserves careful attention and accurate measurement.

It is important to note that for a glassy slag, where a much greater (5x) uncertainty in T_{Fsol} is expected, the sensitivity would increase dramatically, especially for a non-expert in slag microstructural behavior. With such larger uncertainty ranges, the slag phase fractions will vary significantly down the mold, which would greatly amplify the sensitivity of the heat flux to T_{Fsol}.

Regarding the third parameter, a larger slag viscosity exponent n causes a more gradual increase in viscosity as the liquid slag cools, which leads to higher viscosities between 1300 °C and T_{Fsol}. As the liquid slag viscosity increases, the average velocity of the liquid slag also increases, which tends to decrease the slag-layer thickness, which increases the heat flux. Alternatively, decreasing n has the opposite effect: viscosity stays lower during cooling and suddenly increases, which tends to lower the heat flux. Note that glassy slags tend to have larger n, but lower T_{Fsol}, with a net effect of higher heat flux. Although this parameter had small sensitivities in the current study involving a crystalline slag, it would be more important for glassy slags, especially due to its dependence on other uncertain parameters T_{Fsol} and f_v, which would also change.

7.9. Contact Resistances

As discussed previously, air gaps influence heat transfer in two different places: inside the oscillation marks when the liquid slag runs out, and/or in the surface roughness of the solid slag layer against the mold wall. If the mold experiences problems with insufficient taper, then the corner regions may experience true macroscopic air gaps, which would truly dominate the sensitivity analysis, as discussed previously.[33] This work focusses on behavior down the centerline of the narrowface in a slab caster, which should be in reasonably good contact with the mold.

The contact resistance imposed by the solid slag/mold air gap acts as an insulator to heat conducting out of the steel slab. Naturally, this contact resistance shows a very asymmetric sensitivity. A larger resistance ($+3\sigma$) has a high sensitivity on "just" the heat flux at mold exit, whereas (-3σ) has negligible sensitivity on all outputs, even for a nonexpert user with limited knowledge of how solidified slag-layer roughness is generated, and other interfacial phenomena that affect the air gap. This is because the baseline contact resistance is already so small that its presence has little effect on model results and therefore decreasing the uncertainty further does not improve our ability to predict the thermal behavior. This is significant, because measuring the slag surface roughness, hydrogen content of the gas, and related properties is very difficult. Note that study of slag/mold contact may be important for its effect on solid layer velocity, as discussed previously.

7.10. Steel Thermophysical Properties

Interestingly, uncertainty in the steel properties (ρ_{steel}, Cp_{steel}, k_{steel}, CTE_{steel}) was found to have negligible contribution to variability of the CON1D model predictions. This low sensitivity of the heat-transfer outputs of interest to the uncertainty in steel properties can be attributed to the low aleatoric uncertainty rising from the relatively accurate measurement methods used to find these parameters (Table 3). The sole exception is the latent heat

(L_f) which showed a small but non-negligible sensitivity for the shell thickness despite a similar uncertainty to the other steel properties. This is because conduction of the latent heat through the solidifying steel has some influence on heat transfer, although the interfacial gap is the rate-limiting step. Furthermore, the low sensitivity of the other steel thermal properties which drive Equation (2) confirms that conduction inside the steel shell is less important than the interfacial gap.

It is important to note that these findings apply only to a plain, low-carbon steel for a single set of casting conditions in a thin-slab caster. Further analysis should be done to investigate the effect of steel grade, including the important indirect effect of steel mechanical properties on heat transfer through shrinkage, oscillation mark and depression formation, especially for peritectic steels. Considering the importance of the slag rim shape and oscillation marks on heat transfer, dynamic multiphysics models of meniscus phenomena and oscillation mark formation are important to better understand and predict mold heat transfer in continuous casting.

8. Conclusion

The present work applies uncertainty quantification and sensitivity analysis to study heat transfer and solidification parameters in the mold of the continuous casting of steel, using the CON1D model. Using an accurate baseline set of conditions for a commercial thin-slab funnel-mold caster from previous work, and uncertainty ranges established from previous literature, each input parameter was adjusted over its uncertainty range to quantify how it propagated to predictions of heat flux, shell thickness, shell surface temperature, and mold temperatures. These outputs of interest were selected for their importance to breakouts, surface defects and longitudinal cracks forming near the meniscus, transverse cracks forming lower in the mold, and mold life issues, respectively. From this work, the following most impactful conclusions can be drawn: 1) The slag rim shape is the most important parameter affecting peak heat flux at and near to the meniscus. Thus, computational models investigating the dynamics of slag rim formation are useful. Furthermore, the control of liquid level fluctuations and other factors which affect slag rim shape is essential to avoid surface quality problems such as longitudinal cracks which are associated with excessive slag rims; 2) Meniscus heat transfer is also sensitive to the uncertainty in the solid slag thermal conductivity near the meniscus, due to the thick solid slag layers. Solid slag conductivity is also important further down the caster, where the slag layer is also relatively solid and thick. Liquid slag thermal conductivity is also important higher in the mold region, but below the slag rim, where the slag is mostly liquid. The liquid slag thermal conductivity sensitivity decreases down the mold region as the liquid slag layer thickness decreases. Thus, it is important to quantify the slag properties, especially the transition from liquid to solid and the thermal conductivities of these phases; 3) The solid slag velocity has a profound impact on all outputs of interest in this work. Increasing the average velocity of the solid slag layer down the mold wall is associated with a thinner insulating slag layer and consequently higher average heat flux and thicker shell at mold exit. More plant measurements and investigations of this important parameter would enable better predictions of mold heat transfer, and likely lead to steel quality improvements as well; 4) Scale layer formation on the mold cold face acts as a resistance to heat transfer and drastically increases mold temperatures, which may lead to boiling and even less heat removal, deterioration of the mold surface with associated strand quality problems, and decreased mold life. Thus, control of mold water quality is essential to stable caster operation; 5) Solid and liquid-slag thermal conductivities have a significant role in the heat transfer in the interfacial gap between the solidifying steel and the copper mold. While extensive data is available for industrial alloys, very few measurements of slag thermal conductivities exist. Although many measurements have already been made, the modeling and control of heat transfer in continuous casting would benefit from even more accurate measurements of slag thermophysical properties, including the thermal conductivity; 6) The slag viscosity at lower temperatures, as quantified by the solidification temperature and exponent in the viscosity model, showed a high sensitivity, even for a crystalline slag where the uncertainty is lowest (glassy slags would have even higher sensitivity). The slag viscosity at 1300 °C was found to have a negligible sensitivity. Thus, better measurements of the high viscosities measurements found at lower temperatures for different slags used in continuous casting would greatly benefit the accuracy of mold heat transfer predictions from models such as CON1D. Such measurements would also likely have significant benefits in design and control of mold slags for consistent thermal behavior and steel quality; 7) Sensitivity analysis and uncertainty quantification is a useful process to identify the most influential modeling parameters, and in doing so, determine specific research areas most deserving of attention to enable improvements in both modeling and process stability in the plant. Thus, the general approach illustrated in this article should be applied to other numerical models and processes, with their own unique input parameters and outputs of interest.

Acknowledgements

The authors thank Begoña Santillana, Tata Steel for assistance in collecting and providing the original plant data and CON1D runs, in addition to former student Lance Hibbeler, and the original developers and contributors to the CON1D code, Bryant Ho, Guowei Li, David Stone, Ya Meng, Xiaoxu Zhou, Nick Youssef, Avijit Moitra, Ying Shang, Huan Li, Xiaoxu Zhou, Pavan Penumakala, and Zhelin Chen. Support for this research from the Continuous Casting Center at Colorado School of Mines is gratefully acknowledged.

Conflict of Interest

The authors declare no conflict of interest.

Data Availability Statement

The data that support the findings of this study are available from the corresponding author upon reasonable request.

Keywords

CON1D, continuous-casting, model, sensitivity analysis, uncertainty

Received: February 6, 2024
Revised: April 11, 2024
Published online:

[1] World Steel in Figures 2023, https://worldsteel.org/steel-topics/statistics/world-steel-in-figures-2023/ (accessed: May 2024).
[2] B. Salah, M. Zoheir, Z. Slimane, B. Jurgen, *Appl. Soft Comput.* **2015**, *34*, 120.
[3] F. He, L. Zhang, *Int. J. Adv. Manuf. Technol.* **2018**, *95*, 4081.
[4] H. Duan, X. Wang, Y. Bai, M. Yao, Y. Liu, Q. Guo, *Int. J. Adv. Manuf. Technol.* **2020**, *109*, 2707.
[5] M. O. Ansari, J. Ghose, S. Chattopadhyaya, D. Ghosh, S. Sharma, P. Sharma, A. Kumar, C. Li, R. Singh, S. M. Eldin, *Micromachines* **2022**, *13*, 2148.
[6] B. G. Thomas, Q. Yuan, S. Mahmood, R. Liu, R. Chaudhary, *Metall. Mater. Trans. B* **2014**, *45*, 22.
[7] D. Shangguan, S. Ahuja, D. M. Stefanescu, *Metall. Trans. A* **1992**, *23*, 669.
[8] M. L. S. Zappulla, B. G. Thomas, in *IOP Conf. Series: Materials Science and Engineering*, Jönköping, June **2020**.
[9] M. L. S. Zappulla, B. G. Thomas, *Mater. Sci. Forum* **2018**, *941*, 112.
[10] J. K. Brimacombe, K. Sorimachi, *Metall. Trans. B* **1977**, *8*, 489.
[11] J. O. Kristiansson, *J. Therm. Stresses* **1984**, *7*, 209.
[12] X. Gao, S. Yang, J. Li, *Mater. Des.* **2016**, *110*, 284.
[13] M. Long, D. Chen, *Steel Res. Int.* **2011**, *82*, 847.
[14] M. L. S. Zappulla, B. G. Thomas, L. C. Hibbeler, *Metall. Mater. Trans. A* **2017**, *48*, 3777.
[15] M. Kawamoto, Y. Tsukaguchi, Y. Nishida, T. Kanazawa, S. Hiraki, *ISIJ Int.* **1997**, *37*, 134.
[16] J. Resa, M. Moore, X. Zhou, H. Ma, A. K. Silaen, C. Q. Zhou, in *TMS 2020*, San Diego, CA, February **2020**.
[17] Z. Chen, W. Drennan, B. G. Thomas, J. Bentsman, in *AISTech 2019*, Pittsburgh, May **2019**.
[18] B. G. Thomas, *CON1D User Manual Version 16.03.01*, University of Illinois, Urbana, IL **2016**.
[19] J. E. Lait, *MS Thesis*, Department of Metallurgy, The University of British Columbia, Vancouver, Canada **1973**.
[20] J. K. Brimacombe, *Can. Metall. Q.* **1976**, *15*, 163.
[21] B. G. Thomas, *Steel Res. Int.* **2018**, *89*, 1700508.
[22] M. Vynnycky, *Metals* **2018**, *8*, 928.
[23] C. Pfeiler, B. G. Thomas, M. Wu, A. Ludwig, A. Kharicha, *Steel Res. Int.* **2006**, *79*, 599.
[24] P. E. Ramirez-Lopez, P. D. Lee, K. C. Mills, B. Santillana, *ISIJ Int.* **2010**, *50*, 1797.
[25] P. E. Ramirez-Lopez, P. D. Lee, K. C. Mills, *ISIJ Int.* **2010**, *50*, 425.
[26] P. E. Ramirez-Lopez, K. C. Mills, P. D. Lee, B. Santillana, *Metall. Mater. Trans. B* **2012**, *43*, 109.
[27] P. E. Ramirez-Lopez, P. N. Jalali, U. Sjöström, P. G. Jönsson, K. C. Mills, I. Sohn, *ISIJ Int.* **2018**, *58*, 201.
[28] C. Ojeda, J. Sengupta, B. G. Thomas, J. Barco, J. L. Arana, in *AISTech 2006 – Proc. of the Iron and Steel Technology Conf.*, Cleveland, OH, May **2006**.
[29] A. S. M. Jonayat, B. G. Thomas, *Metall. Mater. Trans. B* **2014**, *45*, 1842.
[30] X. Yan, A. Jonayat, B. G. Thomas, in *TMS Annual Meeting, Frontiers in Solidification: An MPMD Symp. in Honor of Michel Rappaz*, Nashville, TN, February **2016**.
[31] J. E. Kelly, K. P. Michalek, T. G. O'Connor, B. G. Thomas, J. A. Dantzig, *Metall. Trans. A* **1988**, *19*, 2589.
[32] J. Lee, H. Han, K. Oh, J. Yoon, *ISIJ Int.* **1999**, *39*, 435.
[33] J. K. Park, B. G. Thomas, I. V. Samarasekera, *Ironmaking Steelmaking* **2002**, *29*, 359.
[34] J. X. Song, Z. Z. Cai, F. Y. Piao, M. Y. Zhu, *J. Iron Steel Res. Int.* **2014**, *21*, 1.
[35] X. Wang, L. Kong, M. Yao, X. Zhang, *Metall. Mater. Trans. B* **2017**, *48*, 357.
[36] F. Du, X. Wang, Y. Liu, T. Li, M. Yao, *J. Iron Steel Res. Int.* **2016**, *23*, 83.
[37] Y. Hebi, Y. Man, Z. Huiying, F. Dacheng, *ISIJ Int.* **2006**, *46*, 546.
[38] Y. Meng, B. G. Thomas, *Metall. Mater. Trans. B* **2003**, *34B* 685.
[39] B. G. Thomas, T. Morthland, *3-D Heat Transfer Analysis of Columbus Slab Casting Mold*, University of Illinois, Urbana, IL **2001**.
[40] B. G. Thomas, B. Ho, G. Li, in *Proc. of the Alex McLean Symp.*, Toronto, Canada, July **1998**.
[41] M. Langeneckert, *MS Thesis*, Mechanical Engineering, University of Illinois, Urbana, IL **2001**.
[42] Y. Meng, B. G. Thomas, *Metall. Mater. Trans. B* **2003**, *34B* 707.
[43] H.-J. Shin, B. G. Thomas, G. G. Lee, J. M. Park, C. H. Lee, S. H. Kim, *Materials Science and Technology (MS&T)*, New Orleans, LA, TMS, Warrendale, PA **2004**.
[44] B. Santillana, B. G. Thomas, A. Hamoen, L. C. Hibbeler, A. Kamperman, W. Van der Kroop, in *AISTech 2007, Steelmaking Conf. Proc.*, Indianapolis, IN, May **2007**.
[45] H. Li, B. G. Thomas, *Continuous Casting Consortium Report 200701*, University of Illinois, Urbana, IL **2007**.
[46] B. Santillana, L. C. Hibbeler, B. G. Thomas, A. Hamoen, A. Kamperman, W. Van Der Kroop, *ISIJ Int.* **2008**, *48*, 1380.
[47] R. B. Mahapatra, J. K. Brimacombe, I. V. Samarasekera, N. Walker, E. A. Paterson, J. D. Young, *Metall. Trans. B* **1991**, *22*, 861.
[48] C. A. M. Pinheiro, I. V. Samarasekera, J. K. Brimacombe, B. N. Walker, *Ironmaking Steelmaking* **2000**, *27*, 37.
[49] J. K. Park, B. G. Thomas, I. V. Samarasekera, U. S. Yoon, *Metall. Mater. Trans. B* **2002**, *33*, 425.
[50] Y. Meng, B. G. Thomas, *ISIJ Int.* **2006**, *46*, 660.
[51] X. Liu, M. Zhu, *ISIJ Int.* **2006**, *46*, 1652.
[52] S. Wells, A. Plotkowski, M. J. M. Krane, *Metall. Mater. Trans. B* **2021**, *52*, 3016.
[53] V. R. Voller, C. R. Swaminathan, B. G. Thomas, *Int. J. Numer. Methods Eng.* **1990**, *30*, 875.
[54] S. Koric, B. G. Thomas, V. R. Voller, *Numer. Heat Transfer, Part B* **2010**, *57*, 396.
[55] C. A. Sleicher, M. W. Rouse, *Int. J. Heat Mass Transfer* **1975**, *18*, 677.
[56] L. C. Hibbeler, M. M. Chin See, J. Iwasaki, K. E. Swartz, R. J. O'Malley, B. G. Thomas, *Appl. Mathe. Model.* **2016**, *40*, 8530.
[57] L. Zhang, S. Yang, K. Cai, J. Li, X. Wan, B. G. Thomas, *Metall. Mater. Trans. B* **2007**, *38*, 63.
[58] I. Marschall, G. Xia, N. Kolbl, *Berg Huettenmaenn. Monatsh.* **2018**, *163*, 23.
[59] S. Sridhar, K. C. Mills, S. T. Mallaband, *Ironmaking Steelmaking* **2002**, *29*, 194.
[60] H.-J. Shin, H.-G. Lee, W.-Y. Choi, S.-M. Kang, J.-H. Park, S.-H. Kim, B. G. Thomas, in *AISTech*, Nashville, September **2004**.
[61] R. Saraswat, A. B. Fox, K. C. Mills, P. D. Lee, B. Deo, *Scand. J. Metall.* **2004**, *33*, 85.
[62] M. Wolf, in *2nd European Conf. on Continuous Casting*, Dusseldorf, June **1994**.
[63] K. Tsutsumi, H. Murakami, S.-I. Nishioka, M. Tada, M. Nakada, M. Komatsu, *Tetsu-to-Hagane* **1998**, *84*, 617.
[64] P. Lundkvist, B. Bergquist, *Ironmaking Steelmaking* **2014**, *41*, 304.
[65] W. L. McCauley, D. Apelian, *Can. Metall. Q.* **1981**, *20*, 247.
[66] M. Persson, M. Gornerup, S. Seetharaman, *ISIJ Int.* **2007**, *47*, 1533.
[67] H. Kobatake, J. Schmitz, J. Brillo, *J. Mater. Sci.* **2014**, *49*, 3541.
[68] S. Sridhar, K. C. Mills, O. D. C. Afrange, H. P. Lorz, R. Carli, *Ironmaking Steelmaking* **2000**, *27*, 238.
[69] J. Cho, H. Shibata, T. Emi, M. Suzuki, *ISIJ Int.* **1998**, *38*, 440.
[70] H. Yoo, C. Park, S. Jeon, S. Lee, G. W. Lee, *Metrologia* **2015**, *52*, 677.
[71] J. D. James, J. D. Spittle, S. G. R. Brown, R. W. Evans, *Meas. Sci. Technol.* **2001**, *12*, R1.

[72] B. Hay, S. Barré, J. R. Filtz, M. Jurion, D. Rochais, P. Sollet, *Inter. J. Thermophys.* **2006**, *27*, 1803.
[73] L. Vozár, W. Hohenauer, *Int. J. Thermophysics* **2005**, *26*, 1899.
[74] F. L. Migliorini, E. H. C. Silva, P. A. Grossi, R. A. N. Ferreira, D. M. Camarano, in *19th IMEKO World Congress Fundamental and Applied Metrology*, Lisbon, Portugal, September **2009**, Vol. *4*, pp. 1556–1559.
[75] M. Akoshima, T. Baba, *Int. J. Thermophys.* **2006**, *27*, 1189.
[76] N. D. Milosevic, G. S. Vukovic, D. Z. Pavicic, K. D. Maglic, *Int. J. Thermophys.* **1999**, *20*, 1129.
[77] R. Razouk, O. Beaumont, J. Hameury, B. Hay, *Therm. Sci. Eng. Prog.* **2021**, *26*, 101130.
[78] P. Pichler, B. J. Simonds, J. W. Sowards, G. Pottlacher, *J. Mater. Sci.* **2020**, *55*, 4081.
[79] A. D. Akimenko, A. A. Skvortsov, *Izv. Vyssh. Uchebn. Zaved., Chern. Metall.* **1958**, *12*, 45.
[80] L. C. Burmeister, *Convective Heat Transfer*, 2nd ed., Wiley, Lawrence, Kansas **1993**.
[81] M. L. Huber, A. H. Harvey, *CRC Handbook of Chemistry and Physics: A Ready-Reference Book of Chemical and Physical Data*, CRC Press, Boca Raton, FL **2017**, pp. 6–252.
[82] K. Yu, H. Zhang, Y. Liu, Y. Liu, *Int. J. Heat Mass Transfer* **2019**, *129*, 1066.
[83] I. Setien-Fernandez, T. Echaniz, L. Gonzalez-Fernandez, R. B. Perez-Saez, M. J. Tello, *Int. J. Heat Mass Transfer* **2014**, *71*, 549.
[84] H. Nakada, M. Susa, Y. Seko, M. Hayashi, K. Nagata, *ISIJ Int.* **2008**, *48*, 446.
[85] H. Ohta, K. Watanabe, K. Nakajima, Y. Waseda, *High Temp. Mater. Processes* **1993**, *12*, 139.
[86] M. R. Ozgu, B. Kocatulum, in *76th Steelmaking Conf.*, Dallas, TX, March **1993**.
[87] M. S. Jenkins, B. G. Thomas, in *80th Steelmaking Conf.*, Chicago, IL, April **1997**.